MICROCOPY RESOLUTION TEST CHART

NATIONAL BUREAU OF STANDARDS

Report No. TC-3037-01
Contract No. N00014-85-C-0050

DTIC FILE COPY

A NEW PUMPJET DESIGN THEORY

by

OKITSUGU FURUYA
WEN-LI CHIANG

TETRA TECH, INC.
630 NORTH ROSEMEAD BOULEVARD
PASADENA, CALIFORNIA 91107

FEBRUARY 1987

DTIC
ELECTE
APR 21 1987
A

Prepared for

DAVID W. TAYLOR NAVAL SHIP
RESEARCH AND DEVELOPMENT CENTER
BETHESDA, MARYLAND 20084

OFFICE OF NAVAL RESEARCH
800 NORTH QUINCY STREET
ARLINGTON, VIRGINIA 22217-5000

87 4 21

Report No. TC-3037-01
Contract No. N00014-85-C-0050

A NEW PUMPJET DESIGN THEORY

by

OKITSUGU FURUYA
WEN-LI CHIANG

TETRA TECH, INC.
630 NORTH ROSEMEAD BOULEVARD
PASADENA, CALIFORNIA 91107

FEBRUARY 1987

Prepared for

DAVID W. TAYLOR NAVAL SHIP
  RESEARCH AND DEVELOPMENT CENTER
BETHESDA, MARYLAND 20084

OFFICE OF NAVAL RESEARCH
800 NORTH QUINCY STREET
ARLINGTON, VIRGINIA 22217-5000

APR 2 1 1987

A

Approved for public release;
distribution unlimited

REPORT DOCUMENTATION PAGE		READ INSTRUCTIONS BEFORE COMPLETING FORM
1. REPORT NUMBER TC-3037-01	2. GOVT ACCESSION NO.	3. RECIPIENT'S CATALOG NUMBER
4. TITLE (and Subtitle) A NEW PUMPJET DESIGN THEORY		5. TYPE OF REPORT & PERIOD COVERED Technical – Theory & Experiment Jan. 1, 1986 – Dec. 31, 1986
		6. PERFORMING ORG. REPORT NUMBER TC-3037-01
7. AUTHOR(s) O. Furuya W.-L. Chiang		8. CONTRACT OR GRANT NUMBER(s) N00014-85-C-0050
9. PERFORMING ORGANIZATION NAME AND ADDRESS Tetra Tech, Inc. 630 N. Rosemead Blvd. Pasadena, CA 91107		10. PROGRAM ELEMENT, PROJECT, TASK AREA & WORK UNIT NUMBERS
11. CONTROLLING OFFICE NAME AND ADDRESS DWTNSRDC Dept. of the Navy Bethesda, MD 20084		12. REPORT DATE February 25, 1987
		13. NUMBER OF PAGES 52
14. MONITORING AGENCY NAME & ADDRESS(If different from Controlling Office) Office of Naval Research 800 North Quincy St. Arlington, VA 22217-5000		15. SECURITY CLASS. (of this report) Unclassified
		15a. DECLASSIFICATION/DOWNGRADING SCHEDULE

16. DISTRIBUTION STATEMENT (of this Report)

Approved for public release; distribution unlimited

17. DISTRIBUTION STATEMENT (of the abstract entered in Block 20, if different from Report)

18. SUPPLEMENTARY NOTES

Sponsored by the Naval Sea Systems Command General Hydrodynamic Research Program and administered by the David W. Taylor Naval Ship R&D Center, Code 1505, Bethesda, MD 20084.

19. KEY WORDS (Continue on reverse side if necessary and identify by block number)

Pumpjet
Streamline Curvature Method
Blade-to-Blade Method
Flow Skewness

20. ABSTRACT (Continue on reverse side if necessary and identify by block number)

The pumpjet is a unique fluid machine which utilizes retarded wake flow and produces high propulsive efficiency such as 90%. The existing pumpjet design method is based on a simple two-dimensional graphic method which was used for pump design. As the demand for the speed of underwater vehicles increased in recent years, the existing design method became inappropriate. Effort has been made to develop a new three-dimensional pump design method by combining a blade-through flow theory with blade-to-blade flow theory. Such a method requires

20. many supporting sub-theories to be developed. The foundation work for the blade-through flow theory, i.e., streamline curvature method, three-dimensional flow mapping technique, as well as two-dimensional cascade theory, has been established in the FY-85 GHR program. During this FY-86 GHR program, the blade-to-blade flow theory with corrections due to the three-dimensionality has been established. Particularly, the flow skewness which escaped many researchers has been found essential for accurate design of pumpjet.

TABLE OF CONTENTS

Page

LIST OF FIGURES

iii

1.0　BACKGROUND

The pumpjet is considered to be one of the most promising candidate propulsors for high speed underwater vehicles and, as a matter of fact, it has recently been employed for MK-48 torpedoes, ALWT--Advanced Light Weight Torpedo (now called MK-50), and other underwater vehicles. The pumpjet superiority over other propulsion devices is represented by two major factors, i.e., high efficiency and quietness.

The pumpjet is one of few fluid devices which positively utilizes retarded wake flow and produces high propulsive efficiency. This peculiar situation may be understood readily by considering the momentum equatin applied to a control volume surrounding an underwater vehicle, fixed to the inertial coordinate system. For a conventional propeller, the velocity of flow coming into a propeller blade is approximately equal to the vehicle speed since the propeller diameter is large enough to enjoy the free stream flow. In order for the propeller to generate an effective thrust, it should accelerate the flow, the ejected flow speed being faster than the incoming flow. It means that a certain amount of the energy imparted on the fluid by the thruster is dumped in the surrounding water. On the other hand, for a pumpjet, the incoming flow velocity is retarded and slower than the free stream velocity. In order to generate a thrust, again this flow has to be accelerated. However, if the pumpjet is properly designed, the accelerated flow velocity can be almost the same as the vehicle speed. The ejected flow out of the pumpjet has little relative velocity and thus leaves hardly any jet wake behind the vehicle. Compared to a vessel with a conventional propeller, a vehicle with a pumpjet generates much less wasted energy in the flow field. This is the major reason why the pumpjet can produce a high propulsive efficiency such as 90% or higher when it is properly designed.

1

Quietness is a guaranteed aspect with the pumpjet. As can
be seen from its configuration (Figure 1-1), a long shroud
completely surrounding the rotor helps prevent rotor noise
from emitting into the outside flow field. Furthermore,
this "internal" flow machine has better resistance charac-
teristics against cavitation, resulting in quieter shallow
water operation where propulsors are most susceptible to
cavitation.

However, in order to achieve such a high standard of perfor-
mance, there are many penalties to be paid in reality. The
first such penalty naturally stems from the pumpjet's util-
izing the velocity-retarded wake flow. A typical meridional
flow distribution at the inlet of pumpjet rotor is shown in
Figure 1-2; the velocity at the hub is only 30% of the free
stream velocity and rapidly increases to 75% at the shroud
internal boundary. This large velocity gradient in the
transverse direction is, of course, built up by the viscous
boundary layer effect and is one of the key features causing
difficulties in design, fabrication and eventually in
achieving the pumpjet high performance.

When one designs an axial or a near axial pump, it is cus-
tomary to distribute the blade loading from hub to tip in a
forced vortex or a free vortex distribution method, such as
shown in Figure 1-3. Such distribution methods are impor-
tant in obtaining a nearly uniform discharge jet behind the
rotor in order to minimize the mixing loss. However, a
serious problem arises in attempting to implement either
forced vortex or free vortex loading distribution against
the flow field having a large velocity gradient as shown
in Figure 1-2. Due to the lack of enough meridional flow
velocity near the hub, the blade there should be designed
to have extremely large incidence angle as well as large
camber. It is for this reason that the pumpjet rotor
designed to date has a distorted profile shape from hub to
tip (Figure 1-4). If this were a conventional propeller,

the stagger angle would become smaller towards the hub and the camber would stay more or less constant. However, for the reason mentioned above, the pumpjet blade stagger angle first becomes smaller up to the midspan area but becomes larger toward the hub and thus the camber is designed to be substantially larger.

This unusual rotor blade setup causes various hydrodynamic problems. Since a typical flow incidence angle near the hub has to be extremely high (e.g., 30·), even a slight error in design may cause flow separation, possibly cavitation and then noise generation. Furthermore, even if design is made properly, the same vulnerable situation is generated with a slight flow disturbance or blade deformation due to fabrication inaccuracy[1]. The existing one-dimensional graphic pumpjet design method with empirical corrections for the cascade effect fails to design a pumpjet free of flow separation. The three-dimensional effect due to the diagonal flow configuration and the cascade effect are not properly taken into account. It is for this reason that development of a more accurate three-dimensional pumpjet design theory is in order.

---

[1] Some pumpjet rotors are produced by investment casting process so that the fabrication accuracy cannot be expected to be high.

3

2.0   OBJECTIVES

The objectives of the work under the GHR program are:

1) to develop a more reliable and accurate pumpjet
   design theory based on a three-dimensional pump
   design concept,

2) to accurately incorporate the cascade effect into
   the theory and then,

3) to improve the pumpjet performance characteristics.

The objective of the FY-86 study was to develop a mathematical model for the blade-to-blade flow for the three-dimensional pumpjet design method selected in FY-85. In FY-86, the blade-through flow theory will be incorporated into the blade-to-blade theory, resulting in forming a complete three-dimensional pumpjet design theory.

3.0   THREE-DIMENSIONAL DESIGN METHOD

Design of a pumpjet for an underwater vehicle requires pre-
liminary information on the vehicle including its geometry
and hydrodynamic drag coefficient. Furthermore, most
importantly, the velocity profile at an upstream reference
section should be obtained either analytically or
experimentally. Any error in the velocity profile would
result in a pumpjet of lower efficiency or failure of the
pumpjet meeting the specifications at the design point. In
the present study, it is assumed that this velocity profile
is given at a goal speed or at the corresponding Reynolds
number.

The first step for design of a pumpjet (Figure 3-1) is to
determine the shroud intake diameter. From the viewpoint
of cavitation, the maximum and minimum shroud diameter to
prevent cavitation must exist. If it is too large, the
rotor blade tip speed becomes too high so that cavitation
occurs. On the other hand, if it is too small, the rotation
speed must be increased to generate the required head so
that the chance of cavitation inception also increases.
Another aspect of determining the shroud diameter stems from
the consideration of overall propulsive efficiency. The
equation for global momentum balance should be able to
determine an efficiency-optimum shroud diameter for the
given velocity profile and vehicle drag.

Once the shroud diameter is determined, streamlines will
be calculated by using the streamline curvature method
(SCM). In this calculation, the loading distribution on the
rotor and blade thickness must be assumed in advance. One
of the major concerns in using the existing streamline cur-
vature method lies in the fact that SCM may only be used for
relatively uniform incoming flow, but may generate a sub-
stantial error for a thick wake flow, i.e., highly retarded
flow due to the viscous boundary layer on the vehicle hull.

5

Detailed mathematical formulation and sample calculations have been presented in the 1985 report (Furuya and Chiang, 1986). Also included are discussions regarding the problems of application of conventional SCM to the thick wake flow.

The next step of the design method is to map the stream tube or surface calculated by SCM onto a plane so that the rotor blades are mapped into cascade configuration. If the stream surface is totally cylindrical shape, the governing equation to be used for the cascade analysis will be a Laplace equation. Unfortunately, the stream surface is of three-dimensional cone shape in general for the tail cone section of the underwater vehicle. The field governing equation now becomes a Poisson equation, and the results of powerful potential theory analysis are no more applicable. A method of correcting the effect of the Poisson equation on the potential theory results is introduced to modify the blade profile shape obtained in the potential theory. In choosing the blade profile shape, the experimental data are used to ensure that there is no chance of flow separation due to overloading on the blade. Furthermore, based on the calculated velocity along the blade, the cavitation inception is checked. If there exists a chance of either flow separation or cavitation, the loading distribution from hub to tip should be changed. If such a change is made, and/or thickness of blades is changed, the streamline curvature method should be used again to determine the new location of streamline or stream surface. This iterative procedure is to be repeated until an overall convergent solution is obtained. Section 3.3 describes the technical approach to be used for the blade-to-blade flow analysis. The two-dimensional theory applicable to the mapped stream surface is summarized in Section 3.2. The overall product of three-dimensional pumpjet design is described in Section 3.4.

3.1   BLADE-THROUGH FLOW ANALYSIS - STREAMLINE CURVATURE METHOD

The mathematical formulation for the streamline curvature method (SCM) has been described in the 1985 report (Furuya and Chiang, 1986).

3.2   TWO-DIMENSIONAL ANALYSIS

In the following, the major concept of Mellor's two-dimensional cascade theory will be summarized for the reader's convenience.

3.2.1   Linearized Cascade Theory

A two-dimensional cascade theory is implemented here to be used for calculating the lift coefficient for the three-dimensional flow discussed in Section 3.3. The boundary conditon (Eqn. 3.2-14) has to be modified, as discussed in Section 3.3, when this cascade theory is applied in the quasi three-dimensional flow.

The lift coefficient is determined for any given cascade geometry which is specified by the solidity (blade chord-gap ratio, c/s) and the stagger angle, λ (Figure 3-2). Symbols used in Mellor (1959) were followed; use L_i and C_{L_i} in denoting the ideal lift force and lift coefficient when the drag is zero. Then (see also Weinig, 1964)

$$L_i = (s/c)\rho W_m \Delta V_\theta \qquad (3.2-1)$$

and
$$C_{L_i} = (L_i/c)/(\tfrac{1}{2}\rho W_m^2)$$

$$= 2(s/c)(\Delta V_\theta/W_m) \qquad (3.2-2)$$

where s is the blade pitch, c is the chord length, ρ is the fluid density, W_m is the mean relative velocity, and ΔV_θ is the difference between the peripheral velocity at the exit and that at the inlet.

7

Replacing the product $s\Delta V_\theta$ by the line integral $\oint \overline{v} \cdot d\overline{r}$ on a closed path comprising two streamlines s distance apart and joined by two lines parallel to the θ-direction, we have (Weinig, 1964).

$$C_{L_i} = 2\Gamma/(cW_m) \qquad (3.2-3)$$

where $\qquad \Gamma = \oint \overline{v} \cdot dr \qquad (3.2-4)$

is the circulation around a profile (Wislicenus, 1965).

The camber is assumed to be sufficiently small so that the chord length is substantially equal to the distance measured along the camber line. Then, the circulation around a thin wing profile is given by (Abbott and von Doenhoff, 1959)

$$\Gamma = \int_0^C \gamma \, dx \qquad (3.2-5)$$

where γ is the difference in velocity between the suction and pressure surfaces, which is also the strength of the vortex sheet comprising the blade camber line (von Kármán and Burgers, 1963). Therefore, equation (3.2-3) is expressed by

$$C_{L_i} = 2 \int_0^1 (\gamma/W_m) \, d \, (x/c) \qquad (3.2-6)$$

The cambered blade is built up by superimposing vortices on the camber line and a distribution of sources and sinks on the camber line to account for the profile thickness effects. The distribution of source (sink), q, is (Mellor, 1959)

$$q = W_m \, dy_t/dx + d(uy_t)/dx \qquad (3.2-7)$$

where the thickness of blade is denoted by y_t and the induced chord-wise velocity, u, is considered constant along the y-direction within the profile. The second term can be shown to be negligible (Mellor, 1959) and so we have

$$q/W_m = dy_t/dx$$

$$= (t/c)f_t(x/c) \qquad (3.2\text{-}8)$$

where $\quad f_t'(x) = \partial f_t/\partial x \qquad (3.2\text{-}9)$

and the thickness function f_t is defined by

$$y_t/c = (t/c)f_t(x/c) \qquad (3.2\text{-}10)$$

where t is the maximum thickness of the blade.

The camber function f_c is defined by

$$y_c/c = C_b \, f_c(x/c) \qquad (3.2\text{-}11)$$

where y_c denotes the camber distribution and C_b is defined by

$$C_b = 2 \int_0^\pi (dy_c/dx)\cos\theta \, d\theta \qquad (3.2\text{-}12)$$

in which

$$\cos\theta = 1 - 2 \, x/c \qquad (3.2\text{-}13)$$

A blade is approached by a mean velocity W_m at a mean angle α_m. To satisfy the condition that the normal velocity vanishes at the boundary, the flow velocity, together with the induced velocity, should be tangent to the surfaces. Neglecting the thickness effect, the boundary condition at x_0 becomes

$$(W_m \sin\alpha_m + v_0)/(W_m \cos\alpha_m + u_0) = (dy_c/dx)_0$$

$$= C_b \, f_c'(x_0/c) \qquad (3.2\text{-}14)$$

where u_0 and v_0 denote respectively the x- and y-components of the induced velocity at x_0 on the 0th blade with x measured along the chord from the leading edge.

To find the lift coefficient by equation (3.2-6), we assume that γ/W_m may be represented by a trignometric series as (Abbott and von Doenhoff, 1959)

9

$$\gamma/W_m = 2A_0 (1+\cos\theta)/\sin\theta + 4\sum_{n=1}^{\infty} A_n \sin n\theta \quad (3.2\text{-}15)$$

which is zero at the trailing edge of $\theta = \pi$ so that the Kutta condition is satisfied. This distribution of vortices, together with the distribution of sources/sinks shown in equation (3.2-8), may be used to obtain the components of induced velocity, u_0 and v_0. The components of induced velocity are then substituted into equation (3.2-14). With the aid of (von Kármán and Burgers, 1963; Milne-Thomson, 1966)

$$\int_0 \left[\cos n\theta/(\cos\theta - \cos\theta_0)\right] d\theta = \pi \sin n\theta_0/\sin\theta_0$$

$$(n = 0, 1, 2, \ldots) \quad (3.2\text{-}16)$$

the following equation is obtained:

$$\sum_{n=0}^{\infty} A_n g_n = \sin\alpha_m - C_b f_c'(\theta_0) \cos\alpha_m$$

$$+ C_b \sum_{n=0}^{\infty} A_n h_n - \frac{t}{c}(C_b B - T) \quad (3.2\text{-}17)$$

where g_n, h_n, B, and T are defined in Mellor (1959) except that $f_t'(\theta_0)$ should be replaced by $f_t'(\theta)$ in defining T. A_n are the Fourier coefficients to be evaluated.

For a cascade of certain solidity, incident angle, and stagger angle, equation (3.2-17) is used to calculate N coefficients, A_n, based on the camber and thickness at N locations along the chord. This study follows the solution method of Mellor (1959) which greatly reduces the calculation labor when a set of solutions as functions of the solidity and stagger angle is desired.

Equation (3.2-17) is multiplied by $\cos k\theta_0$ and integrated from 0 to π to obtain an equation for numerical integration.

Having the double Fourier integral functions calculated, the cascade coefficients, A_n, were computed. Then the lift coefficient was obtained from

10

$$C_{L_i} = 2\pi(A_0 + A_1) \qquad\qquad (3.2\text{-}18)$$

which is derived by inserting equation (3.2-15) to equation (3.2-6).

3.2.2   Data Analysis

The NACA 65-series experimental data given by Herrig, et al. (1951) are used to do the multiple regression analysis in the present study. The data include the cascade lift coefficient and the design angle of attack. The design angle of attack is a function of solidity and blade camber (Figure 3-3). The lift coefficient is a function of stagger angle, solidity, blade camber, and angle of attack. Among the lift coefficient values, only those associated with the design angle of attack are used in the data analysis.

Based on 28 data points in Figure 3-3, the fourth order polynomial equation of the design angle of attack, α_d, obtained by the multiple regression analysis is

$$\begin{aligned}
\alpha_d = {}& - 1.78681\ \sigma^4 + 0.51975\ \sigma^3 C_b + 0.02078\ \sigma^2 C_b^2 \\
& - 0.06408\ \sigma C_b^3 + 0.01716\ C_b^4 + 7.68063\ \sigma^3 \\
& - 2.50213\ \sigma^2 C_b + 0.30280\ \sigma C_b^2 + 0.01298\ C_b^3 \\
& - 12.95580\ \sigma^2 + 6.54778\ \sigma C_b - 0.30496\ C_b^2 \\
& + 12.87888\ \sigma + 2.78086\ C_b - 2.22656
\end{aligned}$$

$$(3.2\text{-}19)$$

where σ denotes solidity and C_b represents the camber. Figure 3-4 shows the correlation between the calculated value from Eqn. (3.2-19) and the experimental data. The mean residual is -0.00002, the standard deviation is 0.04, and the maximum residual is 0.09 degrees which is smaller than the error bound of the original data.

Cascade lift coefficient at the design angle of attack has 79 data as a function of stagger angle, solidity, and camber in Herrig, et al. (1951). Two data at the falling limb, in the figure of lift coefficient vs. angle of attack, are

11

removed from the sample. A total of 77 data is used in the multiple regression analysis. The resultant fourth order polynomial equation is

$$
\begin{aligned}
C_b = {} & 0.00000038594 \; \beta^4 - 1.66604 \; \sigma^4 - 2.74752 \; C_\ell^4 \\
& - 0.000050739 \; \beta^3\sigma - 4.42872 \; \sigma^3 C_\ell - 0.093633 \; C_\ell^3\beta \\
& + 0.0013187 \; \beta^2\sigma^2 - 10.87314 \; \sigma^2 C_\ell^2 - 0.0016033 \; C_\ell^2\beta^2 \\
& - 0.0014369 \; \beta\sigma^3 - 9.83274 \; \sigma C_\ell^3 - 0.000035308 \; C_\ell\beta^3 \\
& - 0.000020018 \; \beta^3 + 8.26201 \; \sigma^3 + 20.91537 \; C_\ell^3 \\
& + 0.0040173 \; \beta^2\sigma + 26.19466 \; \sigma^2 C_\ell + 0.33569 \; C_\ell^2\beta \\
& - 0.11946 \; \beta\sigma^2 + 41.23668 \; \sigma C_\ell^2 + 0.0059786 \; C_\ell\beta^2 \\
& - 0.00080978 \; \beta^2 - 14.15108 \; \sigma^2 - 45.84094 \; C_\ell^2 \\
& - 0.010265 \; \beta\sigma - 47.03403 \; \sigma C_\ell - 0.39504 \; C_\ell\beta \\
& + 0.015917 \; \beta + 13.59117 \; \sigma + 36.29869 \; C_\ell \\
& - 5.23047
\end{aligned}
$$

$$(3.2\text{-}20)$$

The results calculated from this equation are shown as solid lines in Figures 3-5 to 3-8 for different relative flow angle at the blade inlet. Also shown in these figures are discrete data at different conditions. The results from the regression analysis fit well with the data.

3.3 THREE-DIMENSIONAL ANALYSIS – BLADE-TO-BLADE FLOW

This section illustrates the theory and procedure to solve the blade-to-blade flow on each stream surface in an axisymmetric three-dimensional flow environment.

3.3.1 Differential Equations

Under the assumption that an axisymmetric stream surface exists in a rotating machine, from the conservation equation of steady circulation, i.e, $\nabla \times \underline{w} + 2\underline{\omega} = \underline{0}$, the following relation is obtained for the relative flow,

$$
\frac{\partial w_m}{\partial \theta} - \frac{\partial (r w_\theta)}{\partial m} = 2\omega r \frac{\partial r}{\partial m} = 2\omega r \sin\lambda \; , \qquad (3.3\text{-}1)
$$

12

where w_m and w_θ are relative flow velocities in the directions of m and θ, r measures the radial distance, and λ' is the angle of the line tangent to the stream surface at the point of interest made with the axis of rotation (Figure 3-9). The continuity equation for the same stream surface is also written

$$\frac{\partial(b\rho w_\theta)}{\partial\theta} + \frac{\partial(b\rho r w_m)}{\partial m} = 0 \tag{3.3-2}$$

where b is the thickness of stream surface and ρ is the fluid density.

Then, a stream function ψ can be defined by

$$w_\theta = \frac{1}{b\rho}\frac{\partial\psi}{\partial m} , \quad w_m = -\frac{1}{b\rho}\frac{\partial\psi}{r\partial\theta} \tag{3.3-3}$$

Substitution of w_θ and w_m in Eqn. (3.3-3) into Eqn. (3.3-1) yields

$$\frac{\partial^2\psi}{r^2\partial\theta^2} + \frac{\partial^2\psi}{\partial m^2} + \frac{1}{r}\frac{\partial r}{\partial m} - \frac{1}{b}\frac{\partial b}{\partial m}\frac{\partial\psi}{\partial m} = -2b\rho\omega\sin\lambda' \tag{3.3-4}$$

3.3.2   Transformation

Consider a Cartesian coordinate system (X,Y) with the origin O at the leading edge of a blade and the X-axis in the axial direction (Figure 3-2), the three-dimensional axisymmetric stream surface given by Eqn. (3.3-4) can be mapped onto this two-dimensional X-Y plane by the following mapping functions

$$\frac{dX}{dm} = \frac{r_0}{r} , \quad \frac{dY}{d\theta} = -r_0 , \tag{3.3-5}$$

where r_0 is an arbitrary constant which is used for the purpose of scaling between the physical coordinate space and mapped plane (X,Y). By using Eqn. (3.3-5), the governing equation (3.4-4) can now be written in the (X,Y) coordinate system as

13

$$\nabla^2 \psi = -2b\rho\omega \left(\frac{r}{r_0}\right)^2 \sin\lambda$$

$$+ \frac{1}{b\rho} \left\{ \frac{\partial(b\rho)}{\partial X} \frac{\partial\psi}{\partial X} + \frac{\partial(b\rho)}{\partial Y} \frac{\partial\psi}{\partial Y} \right\}. \qquad (3.3-6)$$

Also, the relative velocities in the X- and Y-directions are given by

(a) $w_X = \frac{1}{b\rho} \frac{\partial\psi}{\partial Y} = \frac{r}{r_0} w_m = \frac{r}{r_0} c_m$

$$(3.3-7)$$

(b) $w_Y = -\frac{1}{b\rho} \frac{\partial\psi}{\partial X} = -\frac{r}{r_0} w_\theta = \frac{r}{r_0} (c_\theta - u)$

where c_m and c_θ are absolute flow velocities along m and θ directions, respectively.

On the mapped plane, the relative flow angles at the inlet and exit of a blade, β_1 and β_2, respectively, are obtained from the equivalent velocity diagram to be

$$\tan \beta_1 = \frac{w_{Y1}}{w_{X\infty}} \qquad (3.3-8)$$

$$\tan \beta_2 = \frac{w_{Y2}}{w_{X\infty}} \qquad (3.3-9)$$

where the subscripts 1 and 2 denote the condition at the inlet and exit, respectively, of a blade, and $w_{X\infty}$ is the mean value of w_{X1} and w_{X2}.

3.3.3 Effects of Streamline Inclination and Meridian Velocity Variation

As seen from Eqn. 3.3-6, the governing equation for the (X,Y) plane is now a Poisson equation instead of the Laplace equation which exists only for a flow on a perfectly cylindrical stream surface with uniform velocity distribution. Therefore, the results obtained from the two-dimensional linear cacade theory should be corrected according to the right-hand side term of Eqn. (3.3-6). It is readily

understood that these right-hand side terms are satisfied by distributing the following vortices, ζ, and sources, μ, on the entire (X,Y) plane

(a) $\zeta = (\nabla \times \underline{w})_{X,Y} = 2\omega \left(\frac{\Gamma}{\Gamma_0}\right)^2 \sin\lambda'$

(3.3-10)

(b) $\mu = (\nabla \cdot \underline{w})_{X,Y} = -\frac{1}{(b\rho)^2} \left\{ \frac{\partial(b\rho)}{\partial X} \frac{\partial\psi}{\partial Y} - \frac{\partial(b\rho)}{\partial Y} \frac{\partial\psi}{\partial X} \right\}$.

By adding the induced velocities calculated from ζ and μ, the blade profile shape or equivalently the camber obtained in the conventional two-dimensional analysis will be corrected. It should be noted that the first term on the right-hand side of Eqn. (3.3-6) arises from non-zero λ', i.e., the stream surface is not parallel to the axis of rotation, whereas the second group of terms is due to the non-uniform thickness of stream surface or tube caused by the variation of meridional velocity. Needless to say, if $\lambda' = 0$ and $b\rho$ is constant, Eqn. (3.3-6) becomes a Laplace equation and thus a two-dimensional linear cascade theory holds.

A method similar to the present one was developed by Inoue and his colleague. In their study (e.g., Inoue, et al., 1980), there exist a few major drawbacks, some of which could potentially lead to a substantial error in the final design. First of all, since they use a two-dimensional linearized cascade theory, the error becomes significant for high solidity and high stagger angle area, i.e., near the hub, although they introduce experimental data in a later step of the analysis. Secondly, their velocity triangle used for determining the incoming flow angle to the blade is in error of the first order since they did not take into consideration the effect of non-cylindrical and variable thickness stream surface. Finally, due to the use of the linearized cascade theory, they failed to obtain the velocity distribution and therefore a boundary layer analysis

15

and cavitation inception analysis are not possible.

With these aspects in mind, effort has been made in the current GHR project to improve the accuracy of the linear cascade theory as well as to avoid the singular behavior of velocity at the leading edge of blade. Detailed discussions on the loading correction and leading edge correction have been presented in the FY '85 Report.

3.3.4 Induced Velocities

If the inclination of stream surface is small such as that in an axial-flow case, an approximation solution of the velocity induced by the distributed vortices (Eqn. 3.3-10a) are obtained by a replaced average vorticity $\bar{\zeta}$ (Inoue, et al., 1979):

$$\bar{\zeta} = \frac{1}{c \cos\lambda} \int_0^{c \cos\lambda} \zeta \, dX$$

$$= \frac{u_0}{c \cos\lambda} \frac{r_2^2 - r_1^2}{r_0^2} \tag{3.3-11}$$

where c is the chord length, u_0 is the speed of blade at the reference radius r_0, and subscripts 1 and 2 indicate the inlet and exit, respectively, of the blade.

Similarly, when the variation of axial velocity is small, the distribution of sources (Eqn. 3.3-10b) is replaced by a uniform distribution:

$$\bar{u} = \frac{\bar{w}_{X2} - \bar{w}_{X1}}{c \cos\lambda}$$

$$= \frac{\Delta w_X}{c \cos\lambda} \tag{3.3-12}$$

where $\bar{w}$ denotes the average relative velocity.

16

Consider another Cartesian coordinate system (x,y) with the origin at O and the x-axis in the chordwise direction, which has a stagger angle λ relative to the axial direction (Figure 3-4). The mean flow velocity along the chord direction is

$$w_{X\infty} = w_{X\infty} \cos\lambda + w_{Y\infty} \sin\lambda$$

$$= w_{X\infty} \cos\lambda (1 + \tan\beta_\infty \tan\lambda). \tag{3.3-13}$$

The induced velocities, relative to $w_{X\infty}$, due to the uniform distribution of vortices, $\bar{\zeta}$, and sources, $\bar{\mu}$, are

$$\frac{v_{\zeta x}}{w_{X\infty}} = \chi \left(\frac{x}{c} - \frac{y}{c} \tan\lambda\right) \frac{\tan\lambda}{1 + \tan\lambda \tan\beta_\infty} \tag{3.3-14}$$

$$\frac{v_{\zeta y}}{w_{X\infty}} = \chi \left(\frac{x}{c} - \frac{y}{c} \tan\lambda\right) \frac{1}{1 + \tan\lambda \tan\beta_\infty} \tag{3.3-15}$$

$$\frac{v_{\mu x}}{w_{X\infty}} = \xi \left(\frac{x}{c} - \frac{y}{c} \tan\lambda\right) \frac{1}{1 + \tan\lambda \tan\beta_\infty} \tag{3.3-16}$$

$$\frac{v_{\mu y}}{w_{X\infty}} = -\xi \left(\frac{x}{c} - \frac{y}{c} \tan\lambda\right) \frac{\tan\lambda}{1 + \tan\lambda \tan\beta_\infty} \tag{3.3-17}$$

where

$$\chi = \frac{\bar{\zeta} c \cos\lambda}{w_{X\infty}}$$

$$= \frac{1}{\Phi} \frac{r_2^2 - r_1^2}{r_o^2} \tag{3.3-18}$$

and

$$\xi = \frac{\bar{\mu} c \cos\lambda}{w_{X\infty}}$$

17

$$= \frac{1}{\Phi} \frac{r_2 \, \overline{w}_{m2} - r_1 \, \overline{w}_{m1}}{r_0 \, u_0} \tag{3.3-19}$$

are streamline inclination parameter and axial velocity variation parameter, respectively, and

$$\Phi = \frac{r_1 \, \overline{w}_{m1} - r_2 \, \overline{w}_{m2}}{2 \, r_0 \, u_0}$$

$$= \frac{w_{\chi\infty}}{u_0} \tag{3.3-20}$$

is a local flow coefficient, with subscript m denoting the meridional component of the velocity.

Eqns. (3.3-14) and (3.3-15) are good only if the streamline inclination is small. Eqns. (3.3-16) and (3.3-17) are obtained by ignoring the blockage effect of blade thickness. In the following discussion, the blockage effect is considered and the induced velocity from the distributed vortices given by Eqn. (3.3-10a) are obtained by solving the Poisson equation

$$\nabla^2 \psi = -2 b \rho \omega \left(\frac{r}{r_0}\right)^2 \sin\lambda \tag{3.3-21}$$

to give the solution

$$v_{\varsigma Y} = u_0 \left[\left(\frac{r}{r_0}\right)^2 - \frac{r_1^2 + r_2^2}{2 r_0^2} \right] \tag{3.3-22}$$

where u_0 is a reference velocity.

The induced velocity due to the distribution of sources given by Eqn. (3.3-10b) is approximated by (Inoue, et al., 1980)

18

$$v_{\mu X} = \frac{1}{K_b} \left(\frac{b_1 \rho_1}{b\rho}\right) - 1 \; w_{X1} - \frac{1}{2}(w_{X2} - w_{X1}) \qquad (3.3-23)$$

with the blockage factor of blade thickness, K_b, put into the consideration.

By decomposing both $v_{\zeta Y}$ and $v_{\mu X}$ into the x and y directions, Eqns. (3.3-22) and (3.3-23), together with (3.3-13), become

$$\frac{v_{\zeta x}}{w_{x\infty}} = \frac{u_0}{w_{x\infty}} \left[\left(\frac{r}{r_0}\right)^2 - \frac{r_1^2 + r_2^2}{2r_0^2}\right] \frac{\tan\lambda}{1 + \tan\beta_\infty \tan\lambda}$$
$$(3.3-24)$$

$$\frac{v_{\zeta y}}{w_{x\infty}} = \frac{v_{\zeta x}}{w_{x\infty}} \bigg/ \tan\lambda \qquad (3.3-25)$$

$$\frac{v_{\mu x}}{w_{x\infty}} = \left[\frac{1}{K_b}\left(\frac{b_1 \rho_1}{b\rho} - 1\right) \frac{w_{X1}}{w_{X\infty}} - \frac{w_{X2} - w_{X1}}{2w_{X\infty}}\right] \frac{1}{1 + \tan\beta_\infty \tan\lambda}$$
$$(3.3-26)$$

and

$$\frac{v_{\mu y}}{w_{x\infty}} = \frac{v_{\mu x}}{w_{x\infty}} \tan\lambda. \qquad (3.3-27)$$

3.3.5 Boundary Condition

The flow approaches the blade by a velocity $v_{x\infty}$ at an angle β_∞ relative to the axis of symmetry. This velocity, together with flow velocities induced by distributed vortices and sources, should satisfy the following condition of flow tangency:

$$\frac{dy_c}{dx} = \frac{w_{y\infty} + w_{\ell y} + v_{\zeta y} + v_{\mu y}}{w_{x\infty} + w_{\ell x} + v_{\zeta x} + v_{\mu x}} \qquad (3.3-28)$$

where y_c denotes the y coordinate of the camber line, and $w_{\ell x}$ and $w_{\ell y}$, respectively, are the x and y components of velocities induced by bound vortices and sources along the chord.

3.3.6 Flow Skewness in Diagonal Contracting Channel

The major goal of the proposed theory is to make corrections of flow stream tube nonuniformness and diagonal flow effects on the two-dimensional axial cascade flow. This is performed within the framework of perturbation method by uniformly distributing vortices, $\overline{\gamma}$, and source/sink, $\overline{\zeta}$, in cascade row, as described in Section 3.3.4. The blade profile shape will be properly modified in order to take $\overline{\gamma}$ and $\overline{\zeta}$ into account. Due to the distribution of uniform vortices and source/sink, the flow skewness problem exists, i.e., the first order effect on the flow incidence angle is generated by such singularity distribution.

As shown in Figure 3-10, the constant vortices, $\overline{\zeta}$, are distributed in a strip over the entire cascade row. The complex potential W for a point vortex $\overline{\zeta}$ placed at z' is expressed

$$W = \frac{i\overline{\zeta}}{2\pi} \ln (z-z')$$ (3.3-29)

and the induced velocities are obtained by taking the deviations of W

$$\dot{u}_\zeta - i\dot{v}_\zeta = \frac{dW}{d\zeta} = \frac{i\overline{\zeta}}{2\pi} \frac{x-x' + iy'}{(x-x')^2+y'^2} \ .$$ (3.3-30)

The induced velocities due to the uniform distribution of vortices over a strip of cascade region are obtained by integration

$$v_\zeta = \int_0^{\ell\cos\lambda} \int_{-\infty}^{\infty} \dot{v}_\zeta \, dx'dy'$$

$$= \int_0^{\ell\cos\lambda} \int_{-\infty}^{\infty} \frac{-\overline{\zeta}}{2\pi} \cdot \frac{x-x'}{(x-x')^2+y'^2} \, dx'dy'$$

20

$$= \frac{-\bar{\zeta}}{\pi} \int_0^{\ell\cos\lambda} \tan^{-1} \left. \frac{y'}{x-x'} \right|_0^{\infty} dx'$$

As $x \to -\infty$,

$$v_\zeta = \frac{-\bar{\zeta}}{\pi} \int_0^{\ell\cos\lambda} (-\frac{\pi}{2}-0) \, dx' = \frac{\bar{\zeta}}{2} \, \ell\cos\lambda, \qquad (3.3-31)$$

whereas $x \to +\infty$

$$v_\zeta = -\frac{\bar{\zeta}}{2} \, \ell\cos\lambda. \qquad (3.3-32)$$

Therefore, by distributing $\bar{\zeta}$ uniformly as described above, the upstream and downstream flows are equally deviated from the geometric mean flow, w_∞ (see Figure 3-10 again).

On the other hand, a more rigorous mathematical model by Mani and Acosta (1968) will lead to a totally different conclusion. Since this point has been ignored by many researchers, let us review herein the details of Mani and Acosta's work. In their work, the channel contraction was chosen to be of an exponential shape as shown in Figure 3-11. By satisfying the proper boundary conditions, the velocity component in the y-direction due to a point vortex of unit strength at the origin is obtained (see the report of Mani (1966)),

$$v' = \begin{cases} \dfrac{1}{2\pi} \left[\dfrac{x'}{x'^2+y'^2} (1-\frac{1}{2}\alpha b) + \dfrac{\alpha}{8} \ell n \, \dfrac{(2a-x')^2+y'^2}{x'^2+y'^2} \right] & (3.3-33) \\ \qquad\qquad\qquad + 0\,(\alpha^2) \qquad \text{for } x' \le -b \\[2ex] \dfrac{1}{2\pi} \left[\dfrac{x'}{x'^2+y'^2} (1+\frac{1}{2}\alpha a) + \dfrac{\alpha}{8} \ell n \, \dfrac{(x'+2b)^2+y'^2}{x'^2+y'^2} \right] & (3.3-34) \\ \qquad\qquad\qquad + 0\,(\alpha^2) \qquad \text{for } x' \ge a \ . \end{cases}$$

Therefore, the induced velocity due to a distribution of the vortices over a chord length in the cascade configuration is obtained

$$v = \int_{-1}^{1} \gamma(\xi) \sum_{n=-\infty}^{\infty} v' \, d\xi \qquad\qquad (3.3\text{-}35)$$

with $x' = (x-\xi) \cos\lambda$

$\qquad y' = -ns + (x-\xi) \sin\lambda$

$\qquad a = \dfrac{E}{2} - \xi \cos\lambda$

$\qquad b = \dfrac{E}{2} + \xi \cos\lambda,$

$$v = \begin{cases} \displaystyle\int_{-1}^{1} \gamma(\xi) \, \frac{1}{2\pi} \sum_{n=-\infty}^{n=\infty} \left[\left(1-\frac{1}{2}ab\right) \frac{(x-\xi)\cos\lambda}{(x-\xi)^2+n^2s^2-2ns(x-\xi)\sin\lambda} \right. \\[2em] \left. \qquad + \frac{\alpha}{8} \ell n \, \frac{[E-(x+\xi)\cos\lambda]^2+n^2s^2-2ns(x-\xi)\sin\lambda+(s-\xi)^2\sin^2\lambda}{(x-\xi)^2+n^2s^2-2ns(x-\xi)\sin\lambda} \right] d\xi \\[1em] \hspace{10em} \text{as } x \to -\infty \qquad (3.3\text{-}36) \\[2em] \displaystyle\int_{-1}^{1} \gamma(\xi) \, \frac{1}{2\pi} \sum_{n=-\infty}^{n=\infty} \left[\left(1+\frac{1}{2}\alpha a\right) \frac{(x-\xi)\cos\lambda}{(x-\xi)^2+n^2s^2-2ns(x-\xi)\sin\lambda} \right. \\[2em] \left. \qquad + \frac{\alpha}{8} \ell n \, \frac{[(x+\xi)\cos\lambda+E]^2+n^2s^2-2ns(x-\xi)\sin\lambda+(x-\xi)^2\sin^2\lambda}{(x-\xi)^2+n^2s^2-2ns(x-\xi)\sin\lambda} \right] d\xi \\[1em] \hspace{10em} \text{as } x \to +\infty. \qquad (3.3\text{-}37) \end{cases}$$

Let's simplify the first term of the above integration by defining

$$P = \sum_{n=-\infty}^{n=\infty} \frac{(x-\xi)\cos\lambda}{(x-\xi)^2+n^2s^2-2ns(x-\xi)\sin\lambda} \quad .$$

Then

$$P = \sum_{n=-\infty}^{\infty} \frac{(x-\xi)\cos\lambda}{[(x-\xi)-ns\sin\lambda]^2+(ns\cos\lambda)^2}$$

$$= (x-\xi)\cos\lambda \cdot \sum_{n=-\infty}^{\infty} \frac{1}{(x-\xi)+ins\,e^{i\lambda}} \cdot \frac{1}{(x-\xi)-ins\,e^{-i\lambda}}$$

$$= (x-\xi)\cos\lambda \sum_{n=-\infty}^{n=\infty} \frac{1}{\frac{x-\xi}{e^{i\lambda}}+ins} \cdot \frac{1}{\frac{x-\xi}{e^{-i\lambda}}-ins}$$

$$= \frac{\pi}{2s} \sum_{n=-\infty}^{n=\infty} \left[\frac{1}{\frac{\pi}{e^{i\lambda}}\frac{x-\xi}{s} + in\pi} + \frac{1}{\frac{\pi}{e^{-i\lambda}}\frac{x-\xi}{s} - in\pi} \right]$$

From the identify (see Mellor (1959)),

$$\sum_{n=-\infty}^{n=\infty} \frac{1}{\frac{\pi}{e^{-i\lambda}}\frac{x-\xi}{s}-in\pi} = \coth\left(\pi\frac{x-\xi}{s}e^{i\lambda}\right),$$

then,

$$P = \frac{\pi}{2s}\left[-\coth\left(-\pi\frac{x-\xi}{s}e^{-i\lambda}\right) + \coth\left(\pi\frac{x-\xi}{s}e^{i\lambda}\right)\right] \quad (3.3-38)$$

Therefore,

$$P = \begin{cases} -\dfrac{\pi}{s} & \text{as } x \to -\infty \\[2mm] \dfrac{\pi}{s} & \text{as } x \to +\infty. \end{cases} \quad (3.3-39)$$

The second terms of (3.3-36) and (3.3-37) are defined, respectively

$$Q = \begin{cases} \displaystyle\sum_{n=-\infty}^{\infty} \ell n \; \frac{[E-(x+\xi)\cos\lambda]^2+n^2s^2-2ns(x-\xi)\sin\lambda+(x-\xi)^2\sin^2\lambda}{(x-\xi)^2+n^2s^2-2ns(x-\xi)\sin\lambda} \\[3mm] \hspace{6cm} \text{for } x \leq -1 \\[4mm] \displaystyle\sum_{n=-\infty}^{\infty} \ell n \; \frac{[(x+\xi)\cos\lambda+E]^2+n^2s^2-2ns(x-\xi)\sin\lambda+(x-\xi)^2\sin^2\lambda}{(x-\xi)^2+n^2s^2-2ns(x-\xi)\sin\lambda} \\[3mm] \hspace{6cm} \text{for } x \geq 1 \end{cases} \quad .$$

Then,

$$Q = \begin{cases} \displaystyle\sum_{n=-\infty}^{\infty} \ell n \left[1 + \frac{E^2-2E(x-\xi)\cos\lambda + 4\xi x\cos^2\lambda}{(x-\xi)^2+n^2s^2 - 2ns(x-\xi)\sin\lambda}\right] \\[3mm] \hspace{7cm} , \; x \leq -1 \\[4mm] \displaystyle\sum_{n=-\infty}^{\infty} \ell n \left[1 + \frac{E^2+2E(x+\xi)\cos\lambda + 4\xi x\cos^2\lambda}{(x-\xi)^2+n^2s^2 - 2ns(x-\xi)\sin\lambda}\right] \\[3mm] \hspace{7cm} , \; x \geq 1 \end{cases}$$

23

or

$$Q = \begin{cases} \displaystyle\sum_{n=-\infty}^{\infty} \frac{E^2 - 2E(x+\xi)\cos\lambda + 4\xi x \cos^2\lambda}{(x-\xi)^2 + n^2 s^2 - 2ns(x-\xi)\sin\lambda} & , \quad \text{as } x \to -\infty \\[4mm] \displaystyle\sum_{n=-\infty}^{\infty} \frac{E^2 + 2E(x+\xi)\cos\lambda + 4\xi x \cos^2\lambda}{(x-\xi)^2 + n^2 s^2 - 2ns(x-\xi)\sin\lambda} & , \quad \text{as } x \to +\infty. \end{cases}$$

From (A-11),

$$Q = \begin{cases} \displaystyle -\frac{\pi}{s}\,\frac{E^2 - 2E(x+\xi)\cos\lambda + 4\xi x \cos^2\lambda}{(x-\xi)\cos\lambda} & , \quad \text{as } x \to -\infty \\[4mm] \displaystyle \frac{\pi}{s}\,\frac{E^2 + 2E(x+\xi)\cos\lambda + 4\xi x \cos^2\lambda}{(x-\xi)\cos\lambda} & , \quad \text{as } x \to +\infty, \end{cases}$$

or

$$Q = \begin{cases} -\dfrac{\pi}{s}\,(-2E + 4\xi\cos\lambda) \ , & \text{as } x \to -\infty \\[4mm] \dfrac{\pi}{s}\,(2E + 4\xi\cos\lambda) \ , & \text{as } x \to +\infty. \end{cases}$$

Therefore,

$$v = \begin{cases} \displaystyle\int_{-1}^{1} \gamma(\xi)\,\frac{1}{2\pi}\left[\left(1-\frac{1}{2}\alpha b\right)\left(-\frac{\pi}{s}\right) + \frac{\alpha}{8}\left(-\frac{\pi}{s}\right)(-2E + 4\xi\cos\lambda)\right]d\xi \\ \qquad\qquad\qquad\qquad\qquad\qquad\qquad\qquad , \quad \text{as } x \to -\infty \\[4mm] \displaystyle\int_{-1}^{1} \gamma(\xi)\,\frac{1}{2\pi}\left[\left(1+\frac{1}{2}\alpha a\right)\left(\frac{\pi}{s}\right) + \frac{\alpha}{8}\left(\frac{\pi}{s}\right)(2E + 4\xi\cos\lambda)\right]d\xi \\ \qquad\qquad\qquad\qquad\qquad\qquad\qquad\qquad , \quad \text{as } x \to +\infty \end{cases}$$

Assuming a symmetric loading (i.e., $\displaystyle\int_{-1}^{1}\gamma(\xi)\xi\,d\xi = 0$),

$$v = \begin{cases} \dfrac{\Gamma}{2s}\left[1-\frac{1}{2}\alpha\left(b+\frac{E}{2}\right)\right] \ , & \text{as } x \to -\infty \\[4mm] \dfrac{-\Gamma}{2s}\left[1+\frac{1}{2}\alpha\left(a+\frac{E}{2}\right)\right] \ , & \text{as } x \to +\infty \end{cases}$$

24

where $\Gamma = -\int_{-1}^{1} \gamma(\xi)d\xi$ and $\gamma(\xi)$ is positive in the clockwise direction. If $E = 2a = 2b$,

$$v = \begin{cases} \dfrac{\Gamma}{2s}\left(1 - \dfrac{\alpha}{2}E\right) & \text{as } x \to -\infty \\[2em] \dfrac{-\Gamma}{2s}\left(1 + \dfrac{\alpha}{2}E\right) & \text{as } x \to +\infty \end{cases} \qquad (3.3\text{-}40)$$

Rewriting this induced velocity in two parts, by v_Γ and v_α,

$$v = \begin{cases} v_\Gamma - v_\alpha, & \text{as } x \to -\infty \\[1em] -v_\Gamma - v_\alpha, & \text{as } x \to +\infty \end{cases}$$

where $v_\Gamma = \dfrac{\Gamma}{2s}$, $v_\alpha = \dfrac{\Gamma}{2s} \cdot \dfrac{\alpha}{2}E$.

The velocity diagram is now written in Figure 3-12. It is clearly seen that there exists an error of first order of α if w_∞ is chosen as the reference velocity. Instead, w_∞' should be chosen as the reference velocity so that the blade setting will be changed. This error is substantial since the three-dimensional, diagonal flow correction handled under the current method is order of magnitude α. This fact indicates that not only the blade camber profile needs correction as discussed earlier but also the blade setting should be changed in order to take such 3-D correction into account correctly. Inoue, et al. (1979, 1980) did not see this point in their series of papers.

There exist two possible ways of implementing this idea: 1) by assessing the flow channel contraction or expansion in terms of equivalent α, Equation 3.3-40 will be used, and 2) a more accurate calculation will be made by using the distributed vortices over the cascade strip. The method of actually incorporating this flow "skewness" into the current design theory will be one of the major tasks in the FY-87 GHR project.

3.3.7   Secondary Flow Correction

The secondary flow theory commonly used for axial flow is applicable to the current diagonal flow. The strength of vortex at the exit of blade channel due to the secondary flow, ζ_{SF}, is expressed

$$\zeta_{SF} = \frac{N}{2\pi r_2 \cos\beta_2} \left(\zeta_I \; w_1 \; \frac{b_1}{b_2} \; \oint \; \frac{ds}{w} - \frac{1}{\cos\varepsilon} \frac{d\Gamma}{dq} \right)$$

where   N = number of blades,

         ζ_I = the component of vortex normal to the direction of relative flow on the rotating surface,

        w_1 = relative incoming velocity

        s = line element along the blade on the rotating surface

        w = relative flow velocity on the blade surface

        Γ = circulation of blade

        q = q-line used for the streamline curvature method

        ε = angle of a tangent line of meridional line made with q-line

   b_1, b_2 = widths of flow at inlet and exit, respectively

       β_2 = flow angle at exit relative to chord line.

By distributing the above secondary vortex at the exit of blade channel and satisfying the boundary condition on the hub and casing, the induced flow effect on C_θ (called ΔC_θ hereafter), will be calculated by solving the corresponding Poisson's equation. In the current design problem, this ΔC_θ will be taken into consideration for determining the blade profile shape. More detailed numerical analysis will be developed in future work.

3.4   DESIGN PROCEDURE

The design procedure presented here is based on the assumption that the shape and steady velocity of underwater

vehicle is given. The whole procedure can be repeated for a modified shape or velocity. At the beginning, some parameters, such as the location of the rotor, the number of blades, and rotation speed, have to be chosen based on experiences.

Then (Figure 3-1), the stream curvature method (SCM) is used to determine the streamlines for a through-flow in a meridional plane. As discussed in Section 3.1, the method is based on solving the momentum equation along quasi-orthogonal lines (q-lines) and the conservation of mass is kept along the meridional direction.

After streamlines are determined, average stream surfaces are taken to be the revolution of streamlines about the axis of rotation. Then a program, DSN3, is used to do the remaining design procedure. Figure 3-13 depicts the macro view of the procedure while Figures 3-14 through 3-18 show details of each substep based on the theory presented in Sections 3.1 to 3.3.

Figure 3-14 shows the input data required in the general background. Input data related to each individual cross-section are to be read in Subroutine INP2 as shown in Figure 3-15. Some input data are obtained from the meridional flow solutions computed in the SCM program.

Figure 3-16 shows the subroutine to calculate the flow velocities in the mapped (X,Y) plane as discussed in Section 3.3.2. The subscripts 1 and 2 denote conditions at inlet and exit, respectively, of a blade.

One basic concept in the present design procedure is that the blade camber design based on cascade experimental data is adjusted, by considering the effects of streamline inclination and nonuniform velocity distribution, such that both the final flow turning angle and the incident angle relative to the axis of rotation are the same as those obtained in

27

the two-dimensional flow without the three-dimensional factors.

The camber and turning angle for the case of uniform, parallel flow are evaluated based on the required lift coefficient and solidity (Figure 3-17). The method relies on the experimental data presented in Section 3.2.2.

In the presentation of three-dimensional effects, which are to be considered in the boundary condition as discussed in Section 3.3.5, the camber and stagger angle are adjusted until the turning angle in the mapped two-dimensional plane is the same as that with original camber in the uniform, parallel flow (Figure 3-18). A linearized cascade theory (Section 3.2.1), together with proper boundary condition which has the three-dimensional effects considered (Section 3.3.5), is used to calculate the cascade lift coefficient and the associated total circulation.

If the calculated turning angle for the three-dimensional flow case is different from the desired value, the camber and stagger angles are adjusted in an iteration process until the desired value is achieved to within certain tolerance criterion. When the result is converged, the final camber is the one which, under the influence of three-dimensional flow, will yield the desired lift coefficient.

4.0   CONCLUSIONS

During the FY-86 GHR study, the mathematical model of the blade-to-blade theory for the three-dimensional pumpjet flow has been developed.   The stream surface of nonuniform thickness in the diagonal flow was mapped into plane by a functional mapping function.   The rotor blades now become a row of blades, i.e., cascade configuration.   The Laplace equation in the three-dimensional coordinate system is then converted into a Poisson's equation.   This Poisson's equation is solved as the corresponding Laplace equation combined with the source/sink and vortex distribution on the rotating flow field as a correction.   More specifically, the two-dimensional cascade solution is corrected in terms of blade camber profile shape due to the induced velocities generated by the source/sink and vortex distribution.   An iteration procedure is necessary to satisfy the boundary condition on each blade, namely, the flow tangency condition since the original two-dimensional cascade solution will not satisfy the tangency condition after the correction is made.

An additional important correction due to the correction by the singularity distribution, particularly by the vortex distribution, is that of flow skewness.   It seems that this point was ignored by most researchers, but is as important as the camber correction.   It is of first order of three dimensionality.   This skewness changes the flow directions at upstream and downstream in the same direction so that the blade setting should also be changed.   It means that the stagger angle of the cascade blade should be changed properly.

During the FY-87 GHR study, these two theories, i.e., blade-through flow theory (i.e., Streamline Curvature Method) and blade-to-blade flow theory, will be combined and the iteration procedure will be established.   After developing computer codes, a sample pumpjet design will be attempted.

5.0   REFERENCES

Abbott, I.H., and von Doenhoff, A.E., 1959, Theory of Wing
    Sections, Including a Summary of Airfoil Data,   Dover
    Publications, Inc., New York, NY.

Bruce, E.P., Gearhart, W.S., Ross, J.R., and Treaster, A.L.,
    1974, "The design of pumpjets for hydrodynamic
    propulsion," Fluid Mechanics, Acoustics, and Design of
    Turbomachinery, Part I, NASA SP-304, 795-839.

Furuya, O., and Acosta, A.J., 1973, "A note on the calcula-
    tion of supercavitating hydrofoils with rounded noses,"
    Journal of Fluids Eng., ASME, 95, 221-228.

Furuya, O., and Chiang, W.-L., 1986, "A new pumpjet design
    theory," Report No. TC-3037, Tetra Tech, Inc., Pasadena,
    CA.

Furuya, O., Chiang, W.-L., and Maekawa, S., 1984, "A hydro-
    dynamic study of the ALWT (MK-50) pumpjet," Tetra Tech
    Report TC-3725, Tetra Tech, Inc., Pasadena, CA.

Herrig, L.J., Emery, J.C., and Erwin, J.R., 1951,
    "Systematic two-dimensional cascade tests of NACA
    65-series compressor blade at low speeds", NACA RM L51G31,
    National Advisory Committee for Aeronautics, Washington,
    D.C.

Inoue, M., Ikui, T., Kamada, Y., and Tashiro, M., 1979, "A
    design of axial-flow compressor blades with inclined
    stream surface and varying axial velocity," Bulletin of
    the JSME, 22(171), Paper No. 171-4, 1190-1197.

Inoue, M., Ikui, T., Kamada, Y., and Tashiro, M., 1980, "A
    quasi three-dimensional design of diagonal flow impellers
    by use of cascade data," IAHR Symposium 1980, Tokyo,
    403-414.

Mani, R., 1966, "Quasi two-dimensional flows through
    cascades," Ph.D. Thesis, California Institute of
    Technology, Pasadena, CA.

Mani, R., and Acosta, A.J., 1968, "Quasi two-dimensional
    flows through a cascade," Journal of Engineering for
    Power, ASME, 90(2), 119-128.

Mellor, G.L., 1959, "An analysis of axial compressor cascade
    aerodynamics; Part I, Potential flow analysis with
    complete solutions for symmetrically cambered airfoil
    families; Part II, Comparison of potential flow results
    with experimental data", Journal of Basic Engineering, 81,
    362-378 and 379-386.

von Kármán, Th., and Burgers, J.M., 1963, "General aero-
dynamic theory-perfect fluids", In: Durand, W.F. (ed.),
Aerodynamic Theory, Volume II, General Aerodynamic Theory,
Perfect Fluids, Division E, 1-367, Dover Publications,
Inc., New York, NY.

Weinig, F.S., 1964, "Theory of two-dimensional flow through
cascades", In: Hawthorne, W.R. (ed.), Aerodynamics of
Turbines and Compressors, Section B, 13-82, Princeton
University Press, Princeton, NJ.

Wislicenus, G.F., 1965, Fluid Mechanics of Turbomachinery,
Volumes I and II, Dover Publications, Inc., New York, NY.
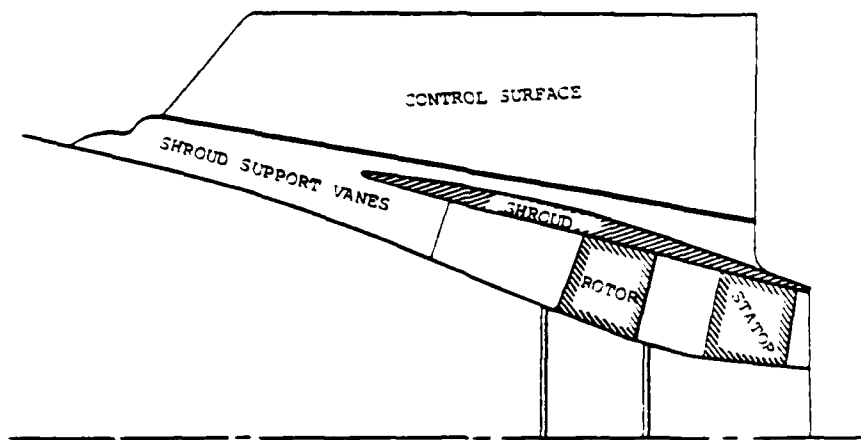
FIGURE 1-1 A typical pumpjet blade and
shroud configuration
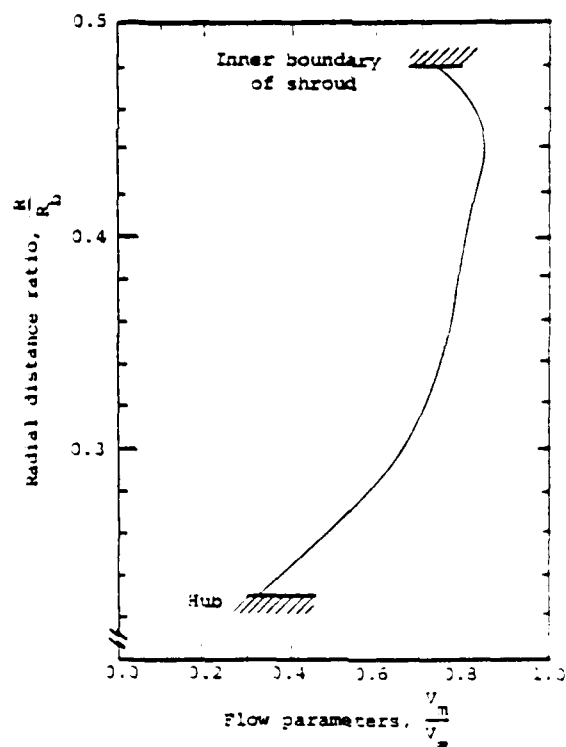
FIGURE 1-2 A typical meridional flow velocity
(V_m) distribution for a pumpjet
where V_∞ is upstream flow velocity

32
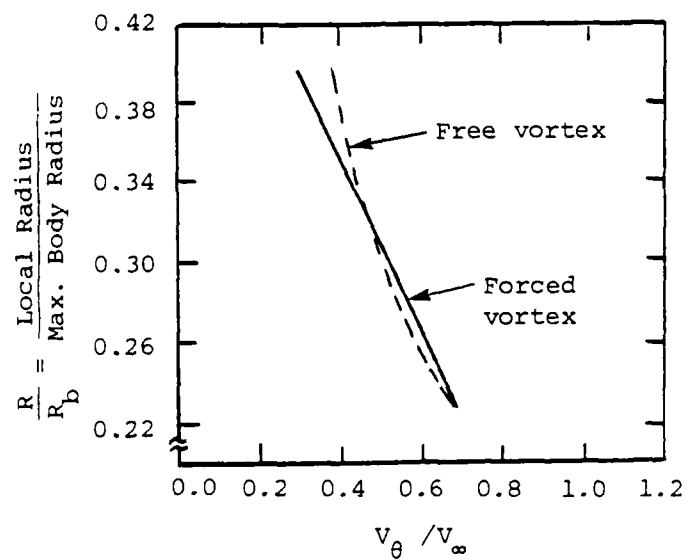
FIGURE 1-3 A typical load distribution
            in terms of V_θ for pumpjet
            rotor blade where V_θ is cir-
            cumferential component of
            the turned flow velocity
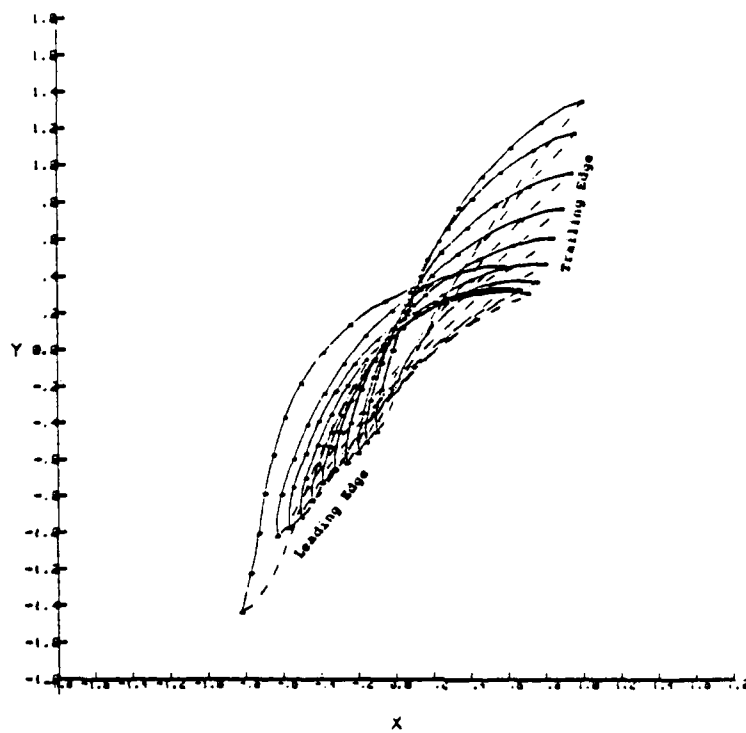
(a)
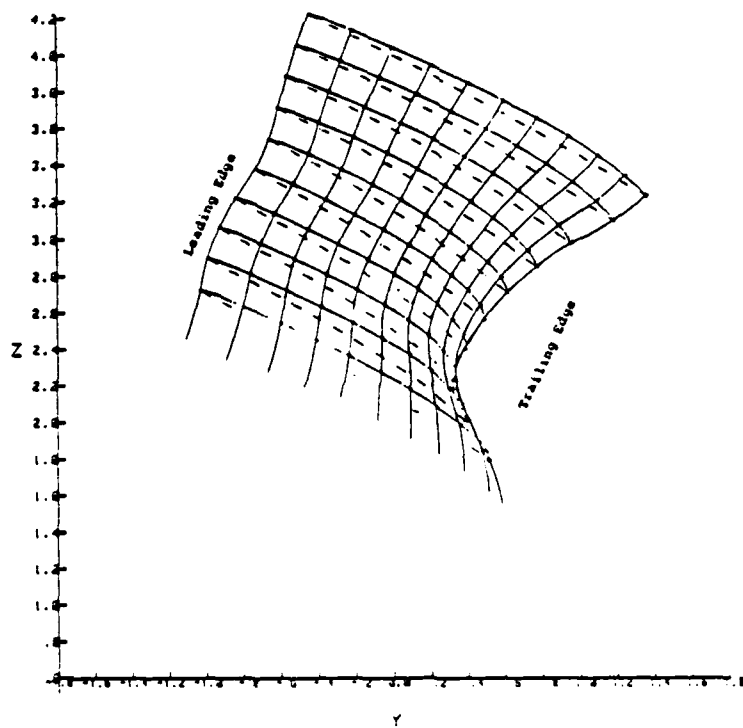
(b)

FIGURE 1-4   Typical pumpjet rotor blade con-
figuration, (a) top view and
(b) upstream view

34
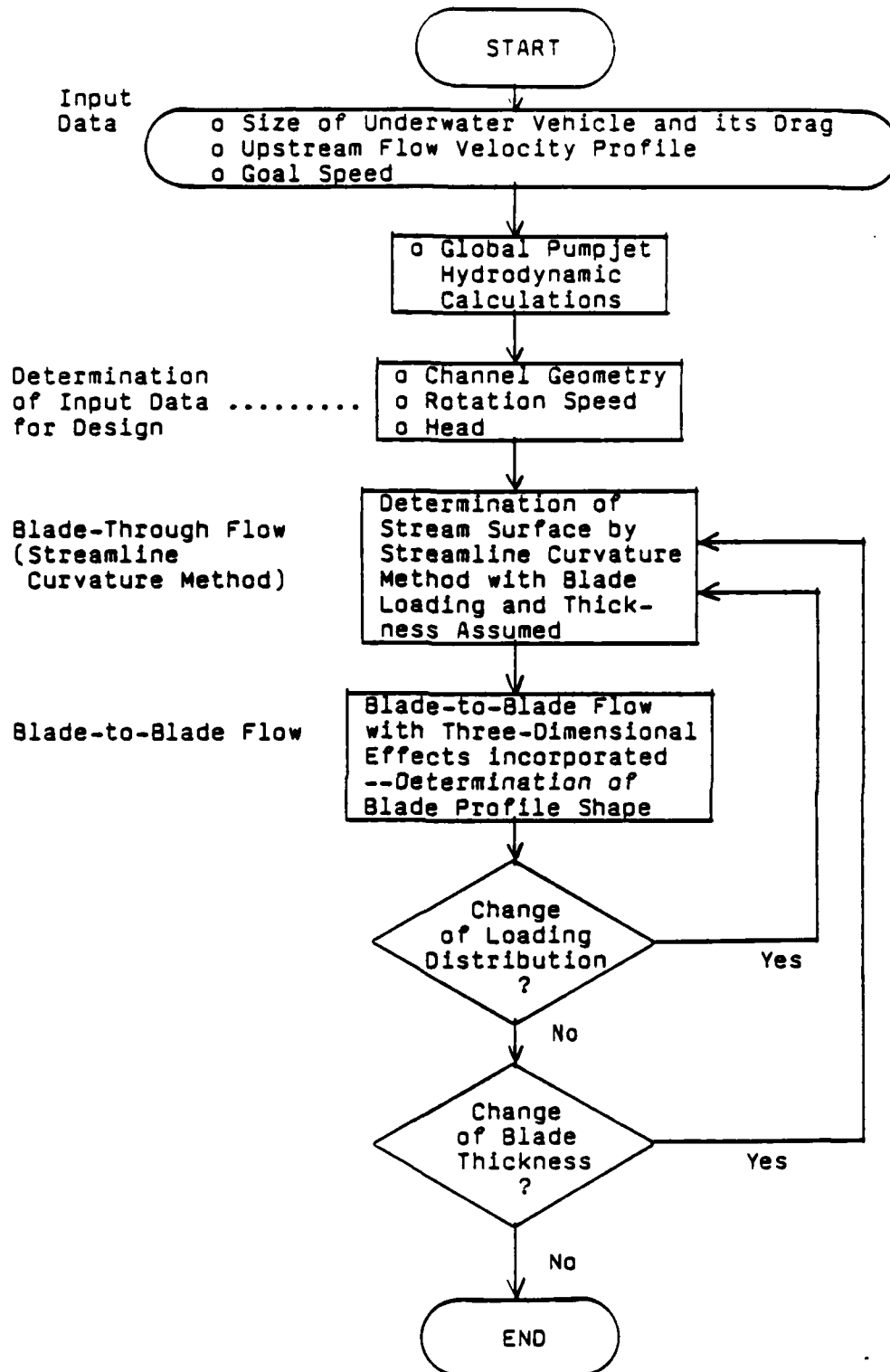
FIGURE 3-1   Flow Chart of the Selected
Pumpjet Design Method

35
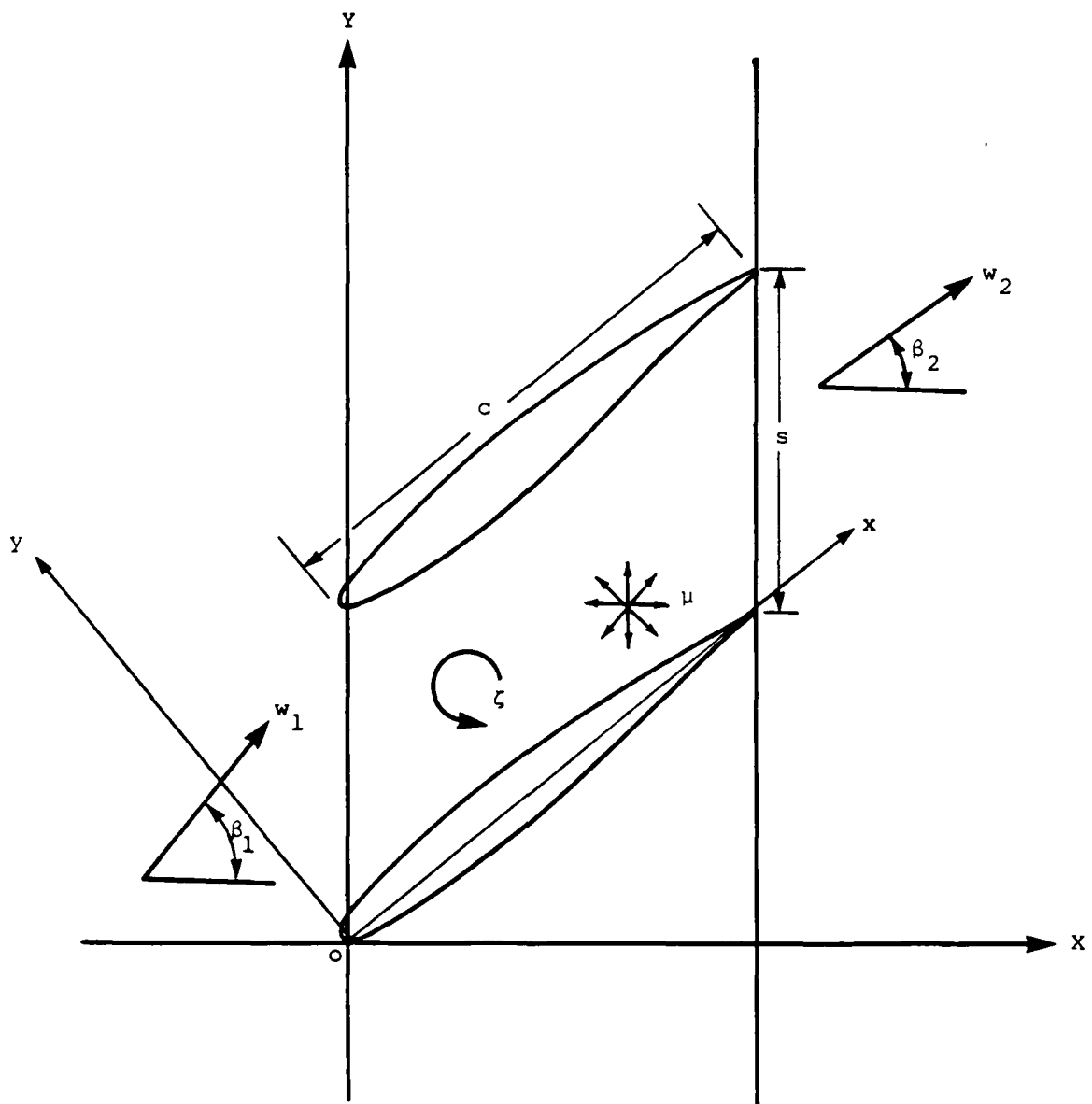
FIGURE 3-2 Definition diagram

36
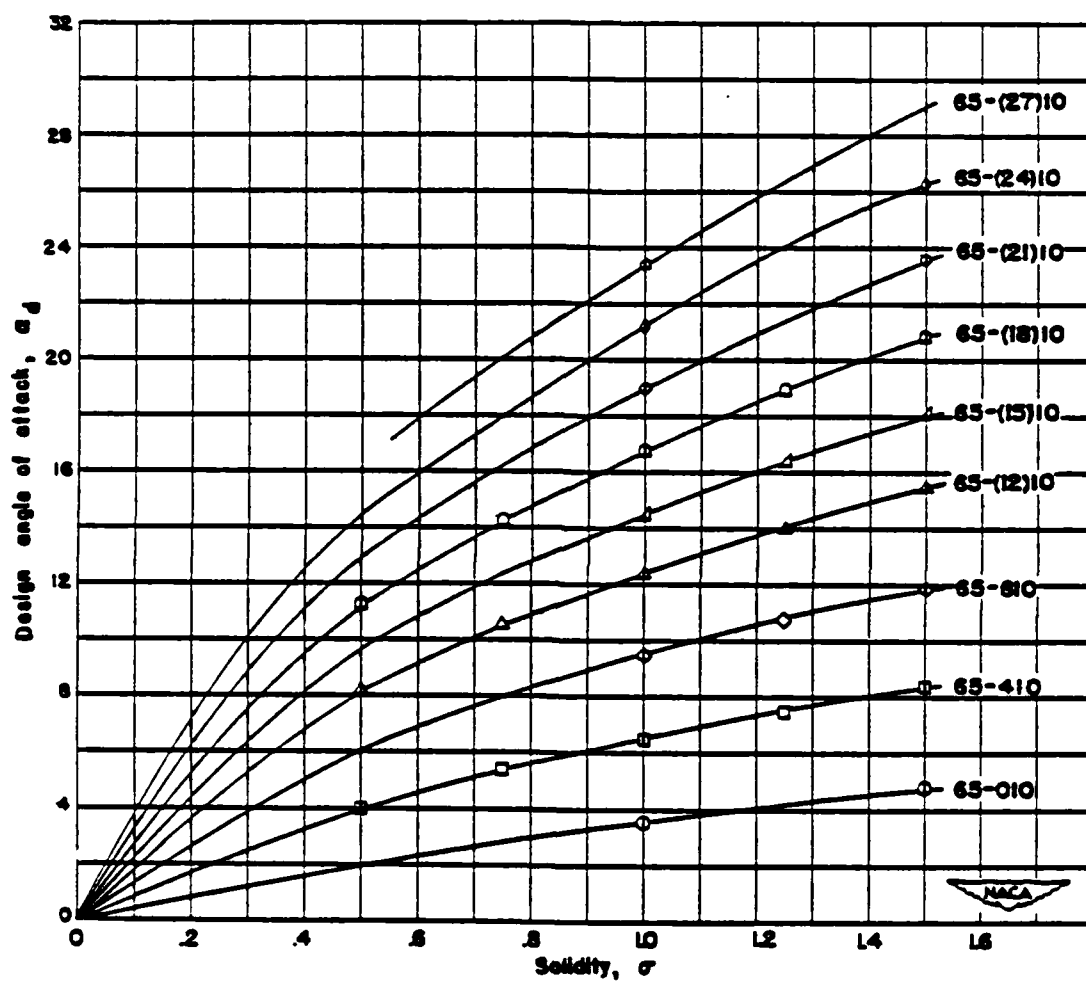
FIGURE 3-3   Variation of design angle of attack with
solidity for the sections tested
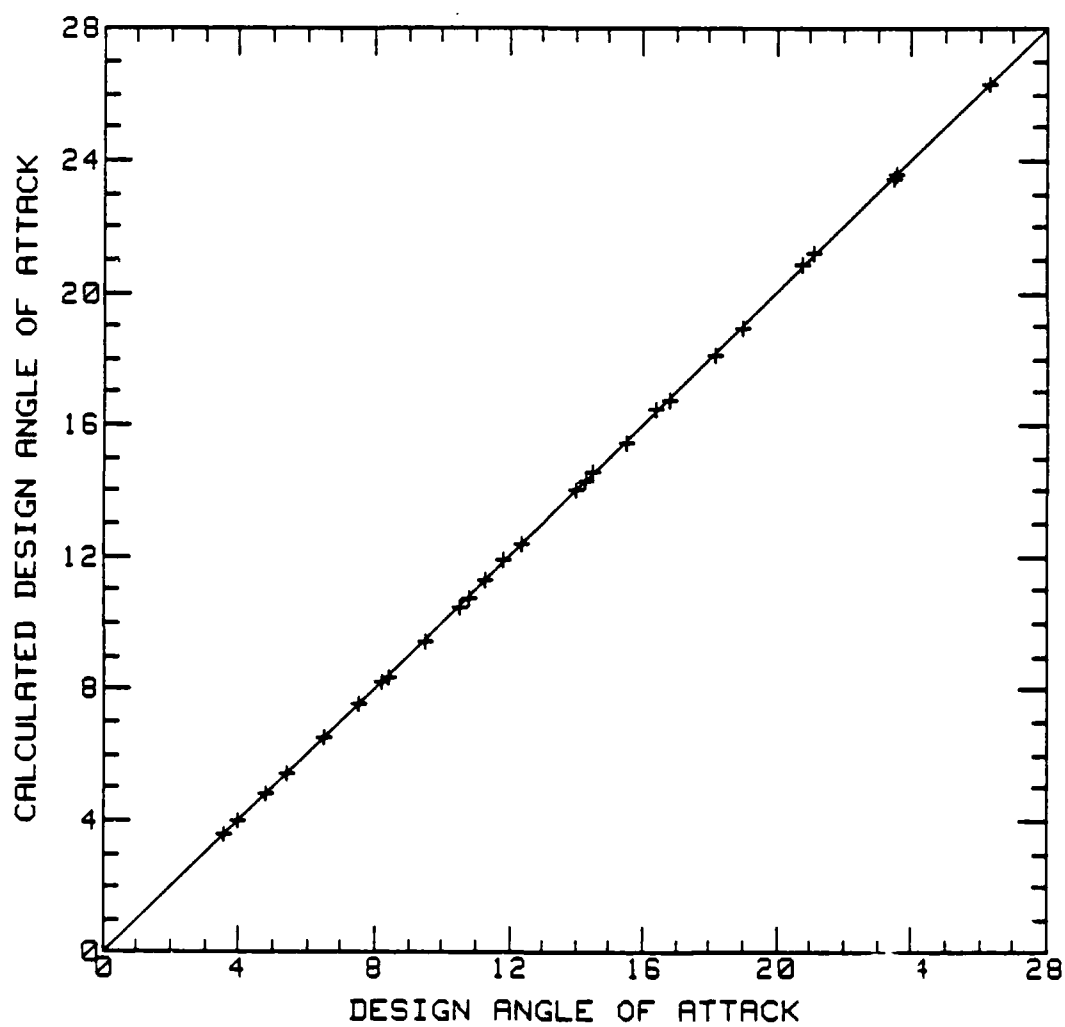
FIGURE 3-4   Comparison of design angle of attack
obtained from the multiple regression
analysis and those obtained from the
laboratory
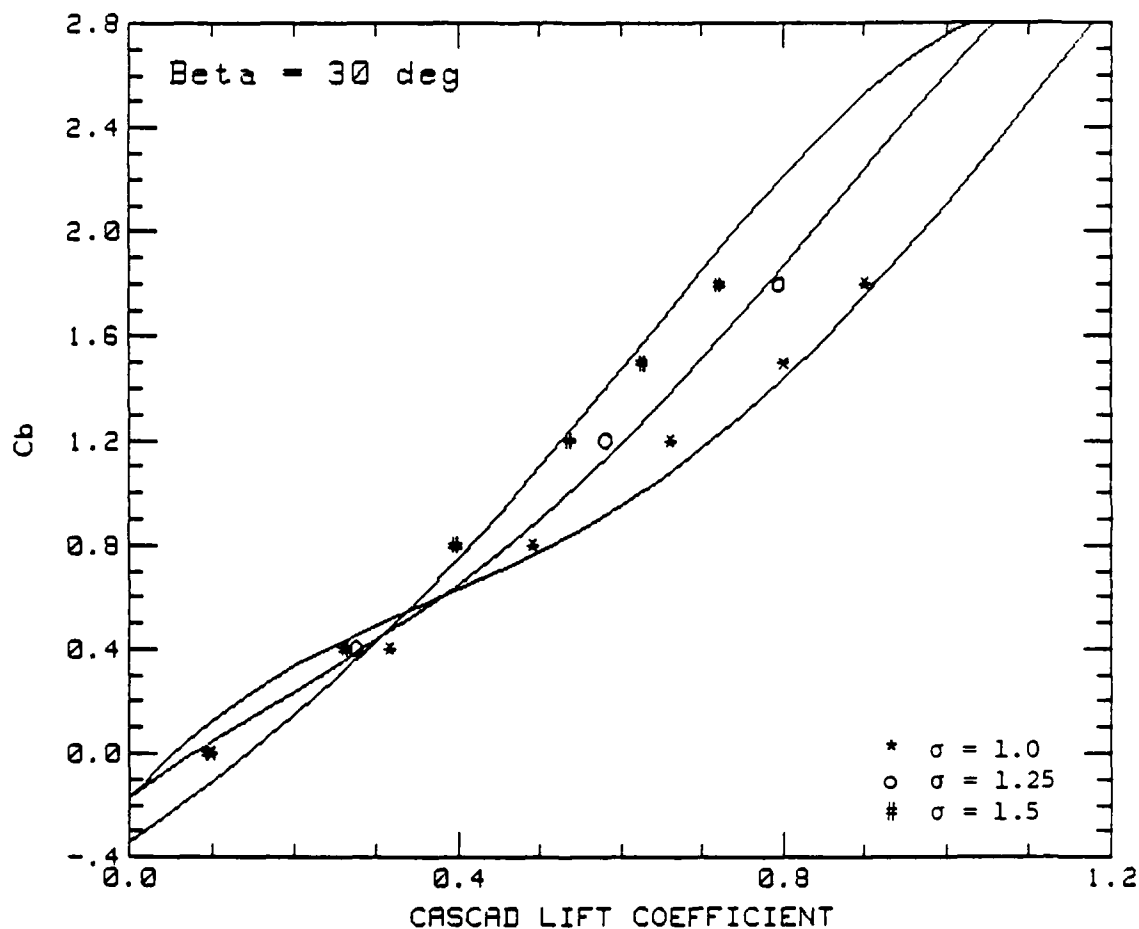
FIGURE 3-5 Camber as a function of cascade lift
coefficient and solidity obtained from
regression analysis data (solid line)
compared with original data (discrete
data point), for $\beta_1 = 30°$
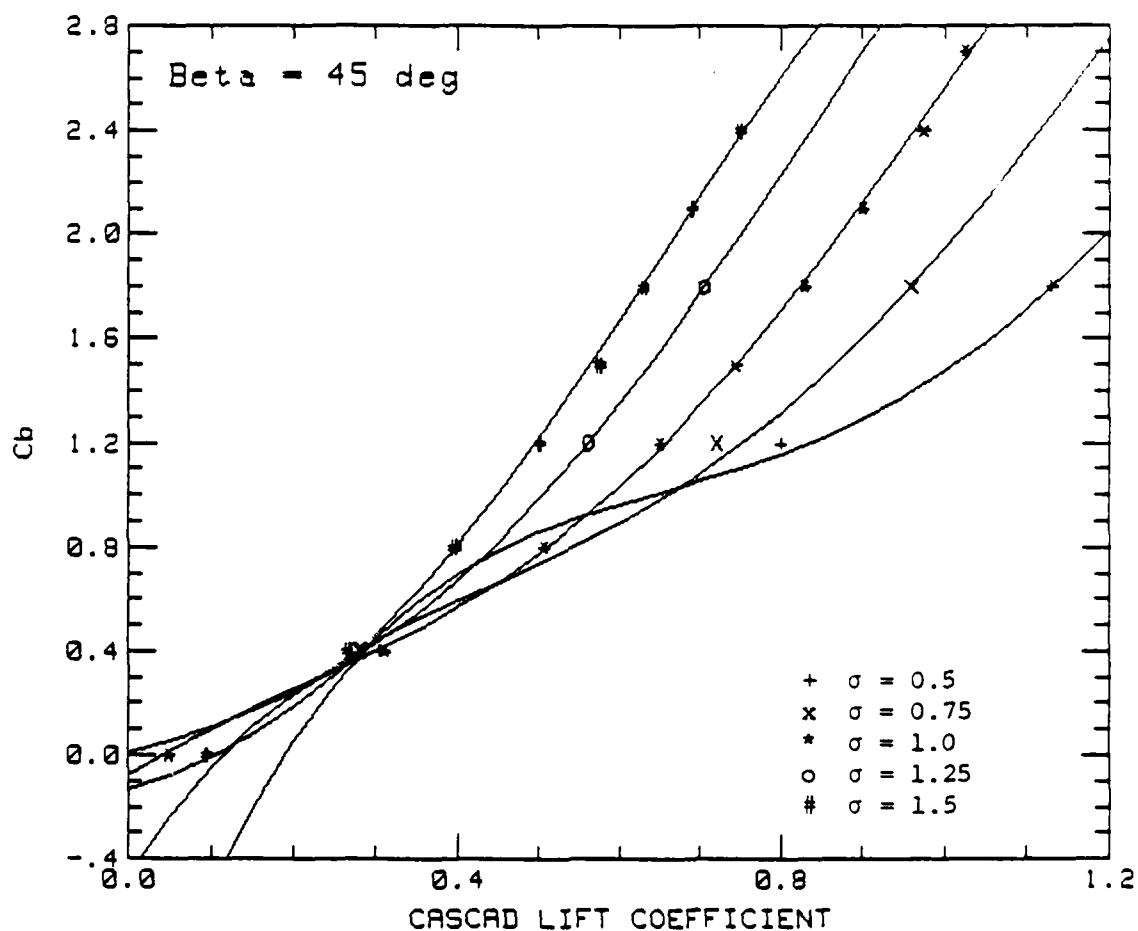
FIGURE 3-6   Camber as a function of cascade lift
coefficient and solidity obtained from
regression analysis data (solid line)
compared with original data (discrete
data point), for $\beta_1 = 45°$

40
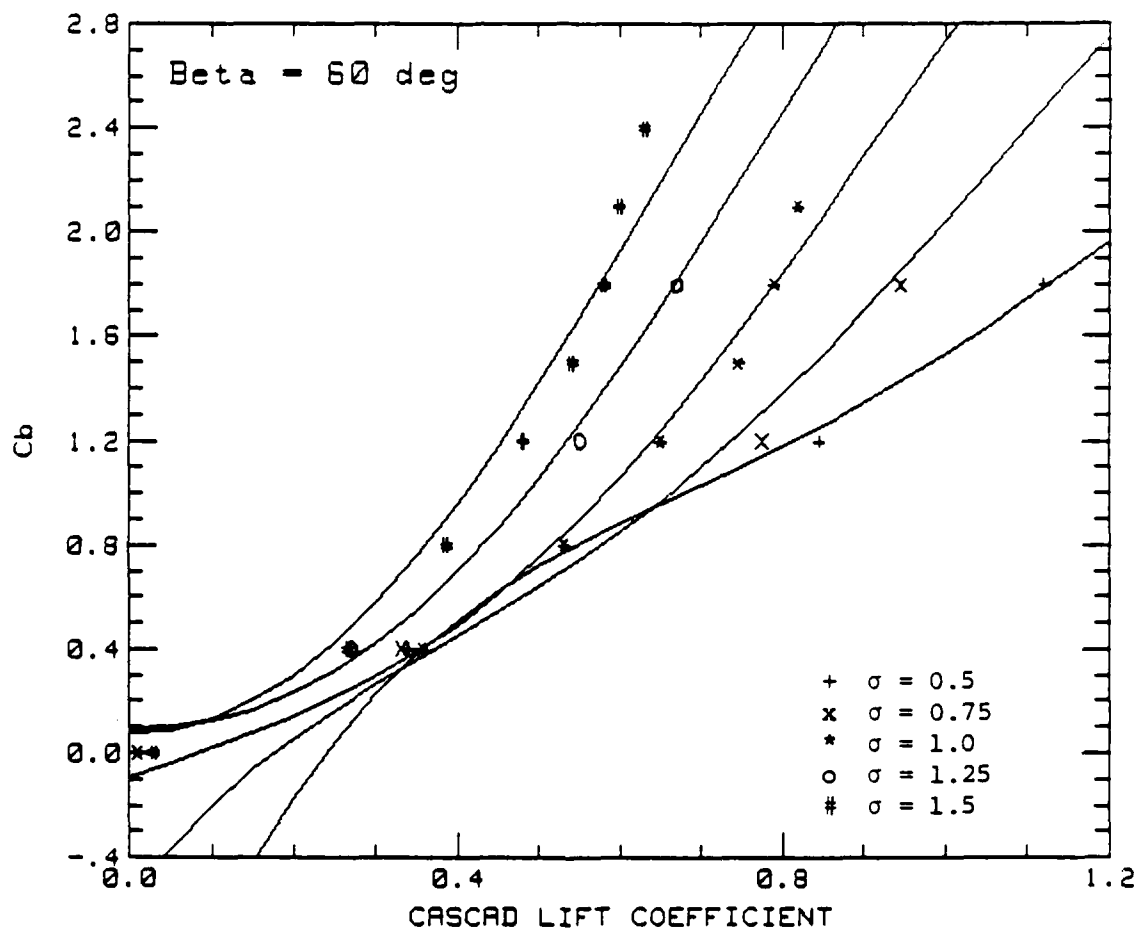
FIGURE 3-7   Camber as a function of cascade lift
coefficient and solidity obtained from
regression analysis data (solid line)
compared with original data (discrete
data point), for $\beta_1 = 60°$

41
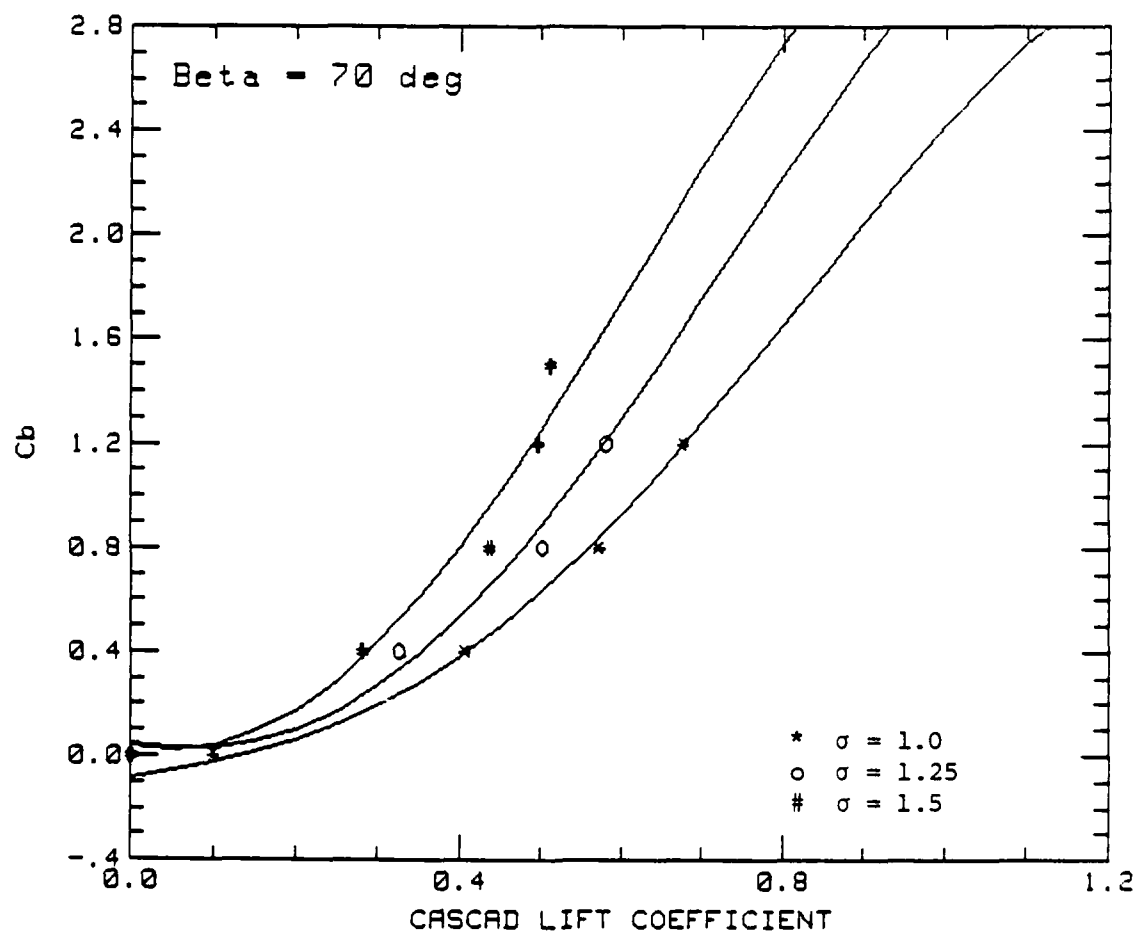
FIGURE 3-8   Camber as a function of cascade lift
coefficient and solidity obtained from
regression analysis data (solid line)
compared with original data (discrete
data point), for $\beta_1 = 70°$

42
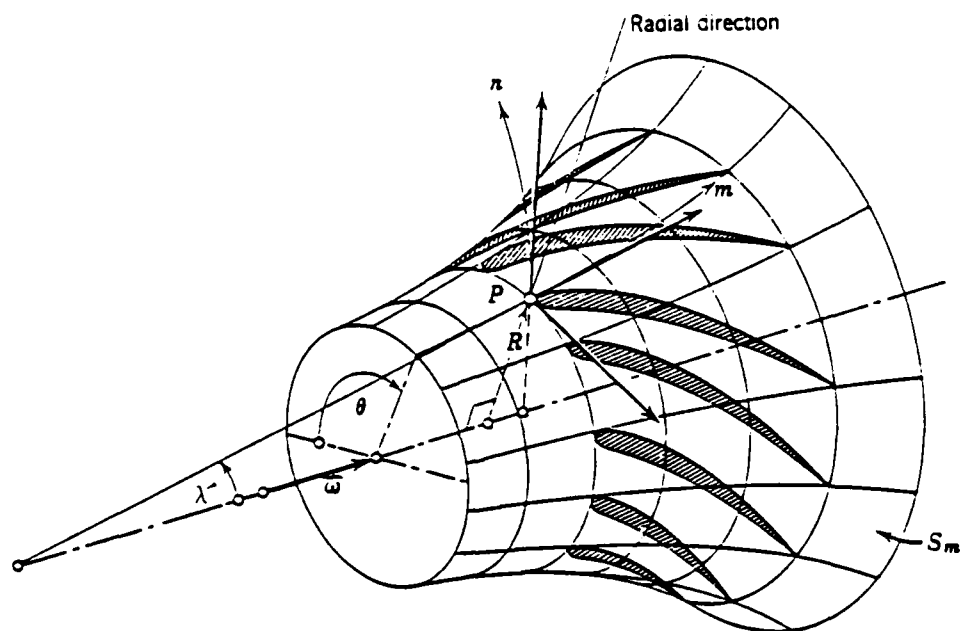
FIGURE 3-9   Axisymmetric stream surface

FIGURE 3-10   Blade setting in the
mapped plane

44
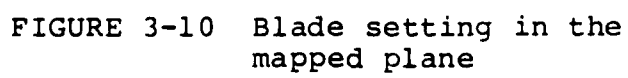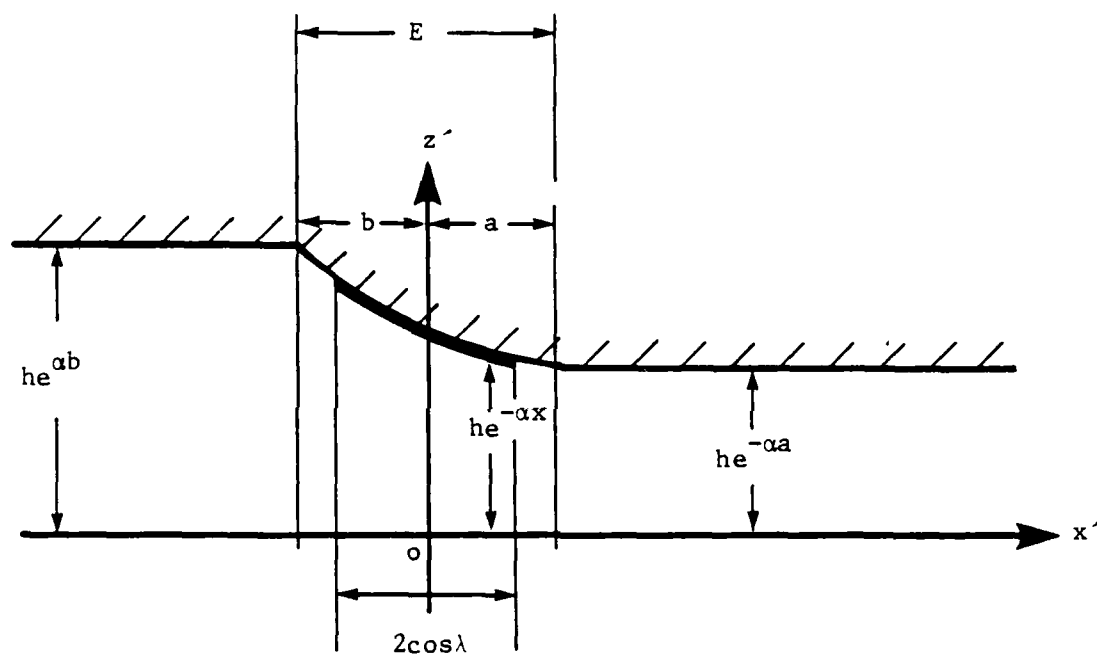
FIGURE 3-11 Flow configuration in
contraction channel
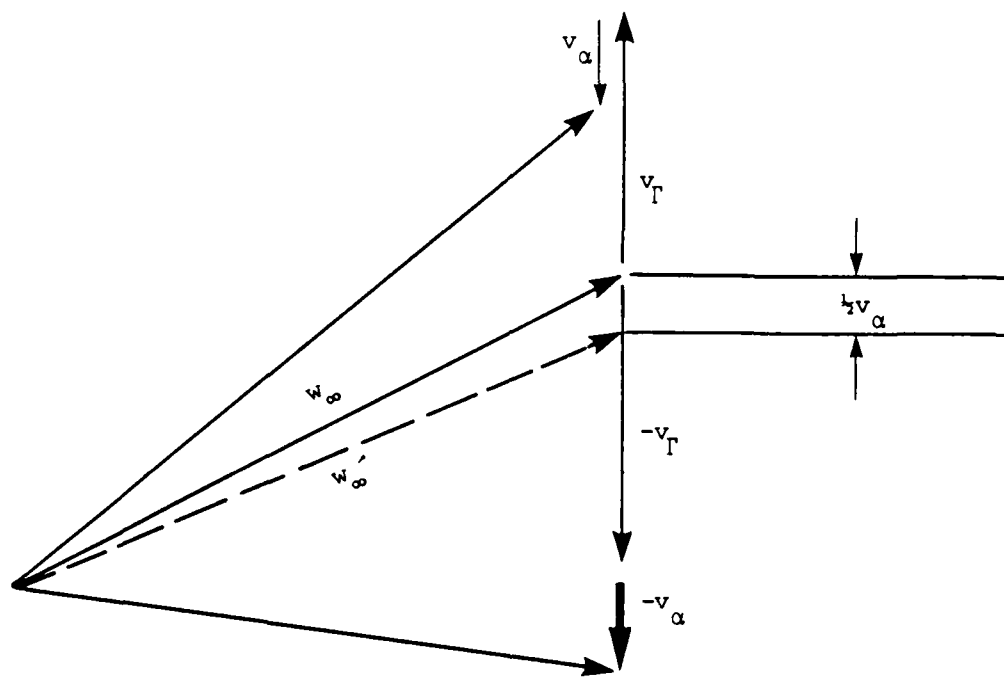
FIGURE 3-12 Flow skewness on the velocity
diagram due to vortex distribution

46

```
                    ┌─────────────────┐
                    │  PROGRAM DSN3   │
                    └────────┬────────┘
                             │
                             ▼
          ┌────────────────────┐         ┌─────────┐
          │  SUBROUTINE INP    │────────▶│  K = 1  │
          └────────────────────┘         └────┬────┘
                             │                 │
                             ▼                 │
          ┌────────────────────┐◀──────────────┘
          │  SUBROUTINE INP2   │◀──────────────────────┐
          └────────┬───────────┘                       │
                   │                                    │
                   ▼                                    │
          ┌────────────────────┐                        │
          │ SUBROUTINE MAP32   │                        │
          └────────┬───────────┘                        │
                   │                                     │
                   ▼                                     │
          ┌────────────────────┐                        │
          │ SUBROUTINE DSN2    │                        │
          └────────┬───────────┘                        │
                   │                                     │
                   ▼                                     │
          ┌────────────────────┐                        │
          │ SUBROUTINE PRM3    │                        │
          └────────┬───────────┘                        │
                   │                                     │
                   ▼                                     │
                  ╱╲                                     │
                 ╱  ╲            No      ┌────────────┐  │
                ╱ K = ╲  ───────────────▶│  K = K + 1 │──┘
                ╲ Ncsec╱                 └────────────┘
                 ╲ ? ╱
                  ╲╱
                   │ Yes
                   ▼
              ┌─────────┐
              │   END   │
              └─────────┘
```
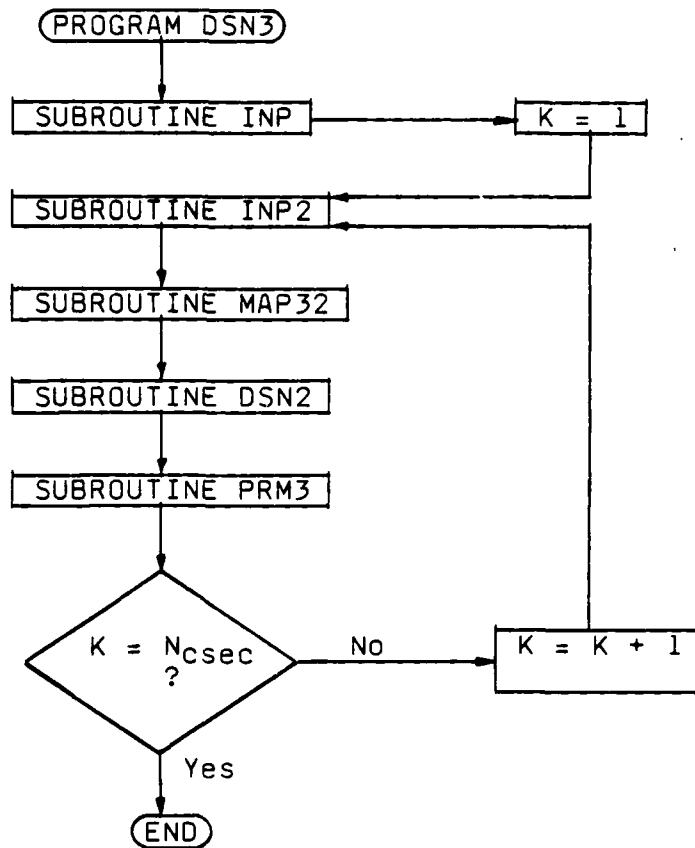
Figure 3-13   General flow chart to design
              blade in a flow of three-
              dimensional character

47

```
                    ( SUBROUTINE INP )
                            |
                            v
┌─────────────────────────────────────────────────────┐
│  Input  Required lift coefficient         C_{\ell o}  │
│                                                       │
│         Flow vel.                         V_∞         │
│                                                       │
│         Rotational speed                  RPM         │
│         Convergence criteria                          │
│            for Δφ_{eq} and Δβ_1          ε_a          │
│                                                       │
│         Max. iteration number            M_{max}      │
│                                                       │
│         No. of blades                    N_{blade}    │
│                                                       │
│         No. of cross-sections along                   │
│            the radius direction          N_{csec}     │
│                                                       │
│         No. of segments along a chord    N_{seg}      │
│                                                       │
│         Ref. radius                      r_o          │
└─────────────────────────────────────────────────────┘
                            |
                            v
┌─────────────────────────────────────────────────────┐
│  For K = 1 to N_{csec}                                │
│                                                       │
│     Input Solidity                       σ(K)         │
│                                                       │
│            Peripheral vel. at inlet      C_{θ1}(K)    │
│            Peripheral vel. at exit       C_{θ2}(K)    │
└─────────────────────────────────────────────────────┘
                            |
                            v
┌─────────────────────────────────────────────────────┐
│ Evaluate angular vel. of rotor, ω, from RPM          │
└─────────────────────────────────────────────────────┘
                            |
                            v
            ┌──────────────────────────────┐
            │  Ref. vel. u_o = r_o ω        │
            └──────────────────────────────┘
                            |
                            v
                      ( RETURN )
```

Figure 3-14   Flow chart for Subroutine INP

```
                    ( SUBROUTINE INP2 )
                              │
                              ▼
┌──────────────────────────────────────────────────────┐
│                                                        │
│  For each cross-section K,                             │
│                                                        │
│     For I = 1 to N_seg,                                │
│                                                        │
│        Input Radius                         r(I)       │
│                                                        │
│           Meridional vel.                   C_m(I)     │
│                                                        │
│           Distance between adjacent                    │
│                         streamlines         b(I)       │
│                                                        │
│           Blockage factor                   K_b(I)     │
│                                                        │
│     Let relative meridional vel.                       │
│               W_m(I) = C_m(I)                          │
│                                                        │
└──────────────────────────────────────────────────────┘
                              │
                              ▼
┌──────────────────────────────────────────────────────┐
│  At the inlet of blade,                                │
│     r_1 ■ r(1),              C_m1 ■ C_m(1)             │
│  At the exit,                                          │
│     r_2 ■ r(N_seg),          C_m2 ■ C_m(N_seg)        │
└──────────────────────────────────────────────────────┘
                              │
                              ▼
                        ( RETURN )
```
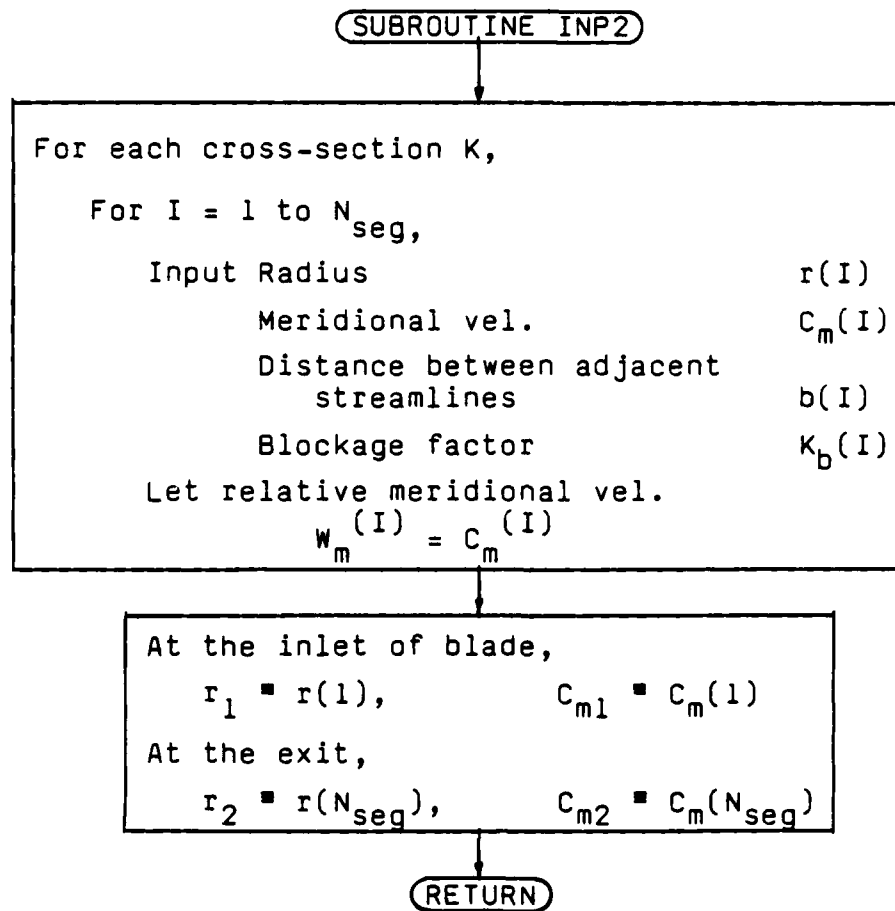
Figure 3-15   Flow chart for Subroutine INP2

```
                    ┌─────────────────────┐
                    │  SUBROUTINE MAP32   │
                    └─────────────────────┘
                              │
                              ▼
        ┌──────────────────────────────────────────┐
        │ Find $w_{X1}$, $w_{X2}$, $w_{Y1}$, $w_{Y2}$, $w_{\theta1}$ │
        │ from Eqn. (3.3-7)                          │
        └──────────────────────────────────────────┘
                              │
                              ▼
        ┌──────────────────────────────────────────┐
        │ Find $w_{X\infty} = \frac{1}{2}(w_{X1} + w_{X2})$ │
        │                                            │
        │ $\Delta w_Y = w_{Y1} - w_{Y2}$             │
        └──────────────────────────────────────────┘
                              │
                              ▼
                        ┌──────────┐
                        │  RETURN  │
                        └──────────┘
```

Figure 3-16   Flow chart for Subroutine MAP32

```
                    ┌─────────────────────┐
                    │  SUBROUTINE DSN2    │
                    └─────────────────────┘
                               │
                               ▼
        ┌────────────────────────────────────────────┐
        │     Determine $\beta_1$ and $\beta_2$ based on │
        │           $\tan \beta = w_Y / w_{X\infty}$     │
        └────────────────────────────────────────────┘
                               │
                               ▼
      ┌──────────────────────────────────────────────────┐
      │  Determine camber $C_b$ and flow angle $\alpha_1$ │
      │      from multiple regression analysis            │
      │    based on experimental cascade data             │
      └──────────────────────────────────────────────────┘
                               │
                               ▼
                    ┌─────────────────┐
                    │     RETURN      │
                    └─────────────────┘
```
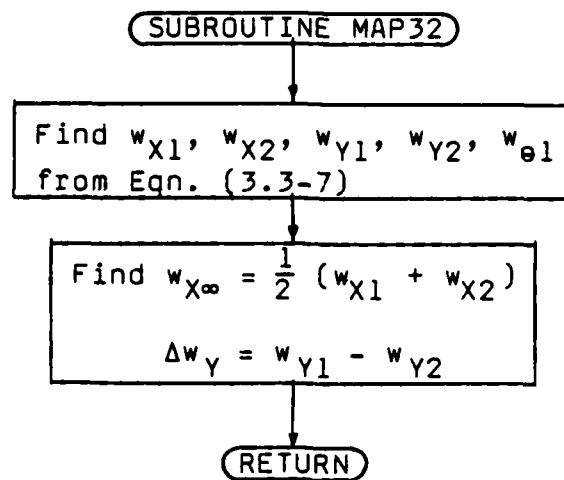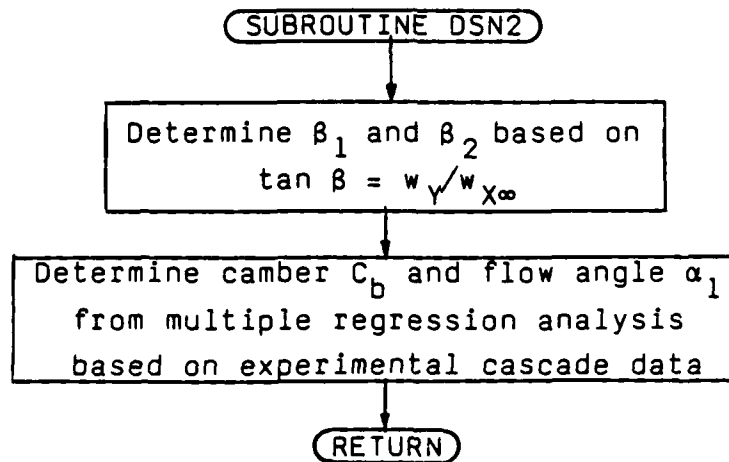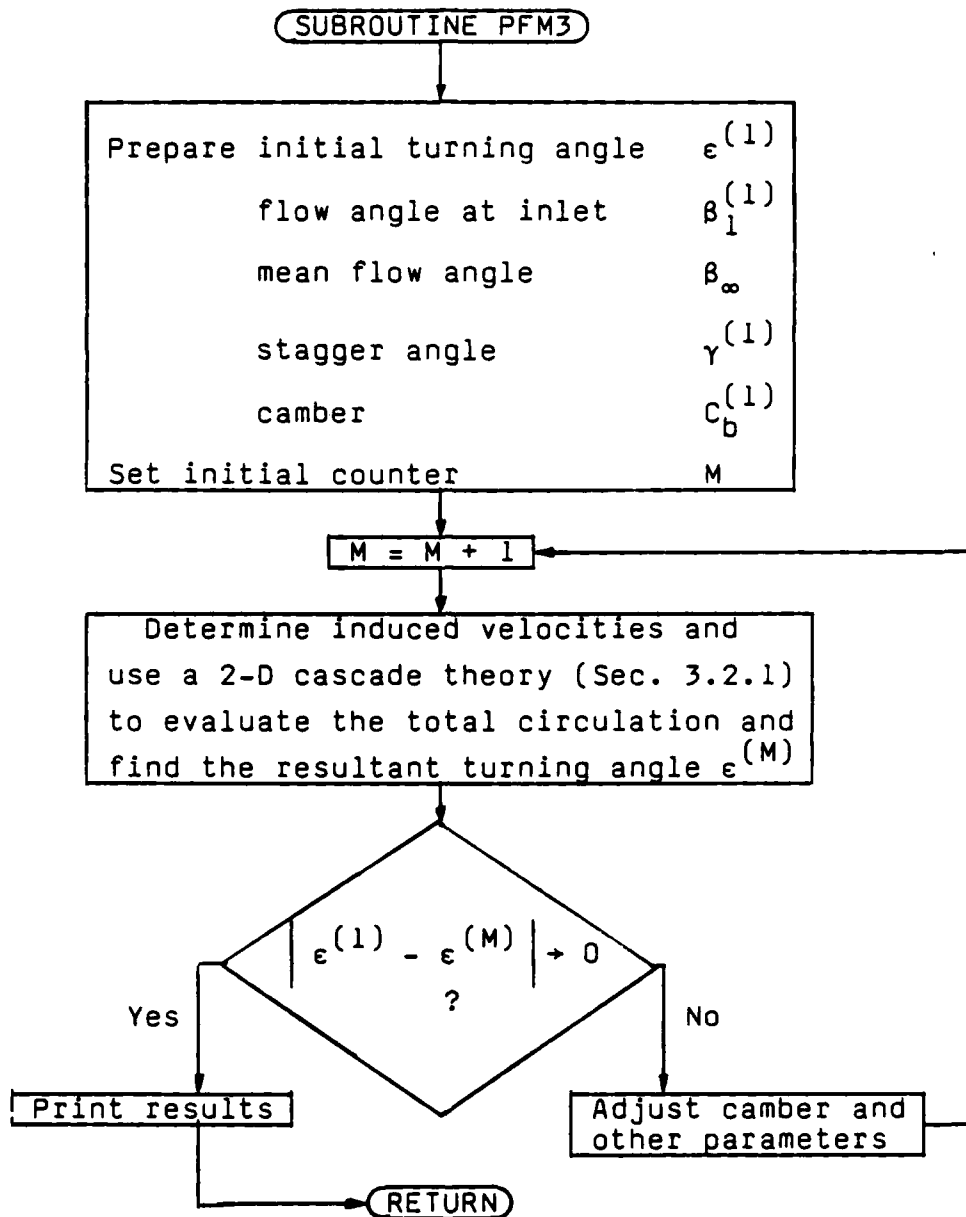
Figure 3-17 Flow chart for Subroutine DSN2

Figure 3-18   Flow chart for Subroutine PFM3

END

5-81

DTIC